POLITECNICO DI TORINO
Repository ISTITUZIONALE

High-speed tracked vehicle model order reduction for static and dynamic simulations

(Article begins on next page)

22 November 2024

High-speed tracked vehicle model order reduction for static and dynamic simulations

Luca Dimauro[*, 1], Simone Venturini [1], Antonio Tota, Enrico Galvagno, Mauro Velardocchia

Department of Mechanical and Aerospace Engineering, Politecnico di Torino, Corso Duca degli Abruzzi, 24, 10129, Torino, Italy

ABSTRACT

In this paper, a model order reduction strategy is adopted for the static and dynamic behaviour simulation of a high-speed tracked vehicle. The total number of degree of freedom of the structure is condensed through a selection of interface degrees of freedom and significant global mode shapes, for an approximated description of vehicle dynamic behaviour. The methodology is implemented in a customised open-source software to reduce the computational efforts. The modelled tracked vehicle includes the sprung mass, the unsprung masses, connected by means of torsional bars, and all the track assemblies, composing the track chain. The proposed research activity presents a comprehensive investigation of the influence of the track chain, combined with longitudinal vehicle speed, on statics and vehicle dynamics, focusing on vertical dynamics. The vehicle response has been investigated both in frequency and time domain. In this last case road-wheel displacements are assumed as inputs for the model, under different working conditions, hence considering several road profiles with different amplitudes and characteristic excitation frequencies. Simulation results have proven a high fidelity in model order reduction approach and a significant contribution of the track chain in the global dynamic behaviour of the tracked vehicle.

© 2024 China Ordnance Society. Publishing services by Elsevier B.V. on behalf of KeAi Communications Co. Ltd. This is an open access article under the CC BY-NC-ND license (http://creativecommons.org/licenses/by-nc-nd/4.0/).

1. Introduction

High-speed tracked vehicles [1,2] are largely used in military, constructive and agriculture sectors, due to their exceptional mobility in harsh conditions and off-road capabilities. In the last decades, different approaches have been deployed by researchers to investigate several aspect of tracked vehicles to simultaneously improve the off-road mobility, ride comfort and Noise Vibration Harshness (NVH) performance. Tracked vehicles have widely different physical and mechanical characteristics with respect to wheeled vehicles. Indeed, wheeled vehicles are more fuel-efficient, offer higher speeds on paved roads with many safety requirements, *e.g.* avoid the rollover risks due to their higher operative speeds or off-road irregularities [3]; Tracked vehicles excel in off-road mobility, reducing ground pressure, which helps them navigate in

challenging environments, thus guaranteeing higher payload capability and versatility. The study of tracked vehicle dynamic behaviour is challenging due to the lack of a deep knowledge about the terrain response to vehicle loading and passage. Therefore, a survey work [4] is proposed, presenting the considerable progress made in the development of analytical approaches for the prediction of tracked vehicle dynamics with a focus on mobility over soft terrain, ride dynamics over rough surfaces and manoeuvrability.

In 1989 Keays research [5] sets out the basis in the calculation of loads applied to the track of a M113 armoured-vehicle in service conditions, in which the performed analysis included the effects of traction load, inertia forces from rotation of the individual shoes, friction, and vibration. The track/wheel-terrain interaction has been mathematically analysed in Ref. [6], combining known constitutive laws for terrain response with a new representation for the track segment, with the aim of running a real-time simulation, which is mandatory for driving simulators. The proposed model allowed the computation of the track tension and the normal and shear forces at the track-terrain interface as the track negotiates terrain of a arbitrary profile. Moreover, a "force" super-element of the track-wheel-terrain interaction has been proposed in Refs. [7,8],

to model the track chain as a belt, through a multibody environment for dynamic simulation of tracked vehicles. Recently, a track dynamic tensioning device is presented together with the design of a neural network-based adaptive controller which is validated against the results obtained with a multibody dynamics environment [9].

Other mathematical models [10] for track representations of varying complexities are formulated in conjunction with an in-plane ride dynamic model of a typical tracked vehicle over rigid terrain profiles. The same authors proposed also a nonlinear model for suspension dynamic analysis and ride quality assessment [11], whereas the ride dynamic behaviour of a high speed vehicle is studied through computer simulations and field tests [12], under the assumption of non-deformable terrain profile. Experimental vehicle test sessions are carried out on discrete half round obstacles of various radii, sinusoidal course, random course, and Belgian Pavé, for various vehicle configurations and speeds. Other experimental activities have been devoted to evaluate the value of forces acting on the tracked vehicle suspension system [13], due to the diversity of their subassemblies material, by means of a genetic algorithm optimization method, which allowed to estimate the damping values of shock-absorbers, or to accurate predict the acceleration and braking performance of the heavy tracked vehicle on both soft and hard terrain [14]. Moreover, nonlinear mathematical models with 17 Degrees of Freedom (DOFs) [15,16] have been built for the ride dynamics of tracked vehicles, validating the nonlinear suspension characteristics with a multibody dynamic model developed in MSC Adams®.

The multibody approach results to be extensively investigated in the last years to achieve a realistic prediction of vehicle dynamics, both in firm and soft soils, with specific attention to the track chain, which plays a key role in transmitting power, providing traction, and influencing the overall vehicle dynamics. The flexibility of track links is analysed in Ref. [17] to evaluate the separate effect of the contact, inertia, and constraint forces associated with the deformation degrees of freedom of the track links, with the aim of comparing the stresses of the track links calculated using the dynamic approach against those obtained using static analysis. Meanwhile, in Ref. [18] compliant force element is used to define the connectivity between the links of the track chains instead of an ideal pin joint. Three-dimensional contact force models are used to describe the interaction of the track chain links with the vehicle components and the ground, demonstrating the significant effect of the bushing stiffness on the dynamic response of the multibody tracked vehicle. Both Experimental Modal Analysis (EMA) with roving hammer test and FEA are performed to evaluate mode shapes of the first 6 modes of the single track. In this context, the influence of single components on the global system, through modal analysis, has been already investigated in Refs. [19,20], using both numerical and experimental approaches and in Ref. [21] where a novel method is proposed to detect the component mode-shapes responsible for undesired dynamics in the assembled multibody systems. A similar approach has been proposed in Ref. [22] for model updating purposes on a vehicular component subject to uncertainties in the mounting process. A multibody dynamic analysis is carried out in Ref. [23], as well, with the aim of determining overall vehicle stability and looking for possible design modifications to improve tracked vehicle performance.

Recalling multibody models, a M113 armored carrier, including chassis, wheel-arms wheels, and track links, is developed in Ref. [24] for dynamic simulation on off-road surfaces, focusing on the description of three-dimensional contact force elements to describe the interaction of the track links with the vehicle's road wheels, sprocket, and idler, whereas additional force elements are used to simulate the bump stops and the dampers. Instead, the commercial software MSC Adams®, together with the Adams Tracked Vehicle Toolkit (ATV) was employed for the multibody modelling of a new passive articulated suspension tracked robot performing a sensitivity analysis on design parameters [25]: after showing a good correlation with experimental data, the digital twin is used to assess the performance of the suspension system in various challenging environments or in accelerated testing conditions. The same software is adopted in Ref. [26] to investigate the dynamic and kinematic behaviour of a tracked machine in several operating conditions, through a novel compact modelling of the tracks—soil interaction in case of soft soil terrains, and in Ref. [27] to predict the robot pose and suspension configuration given the terrain profile. Due to the capability of the model to assess the impact of design parameters, it represents a useful tool to analyze the robot performance or to design the future generations of the rover. Digital twin models have been adopted to predict fatigue failure of automotive components in Ref. [28], showing promising real-time predictive characteristics in experimental accelerated fatigue test conditions, also expanded to driving applications [29].

Other commercial software have been deployed in literature for several purpose, aiming to validate mathematical models, through the use of experimental data, when available:

- Virtual.Lab to simulate the dynamic of a tracked vehicle and specifically to evaluate the displacement courses of characteristic points of the hull and displacements of the wheel axles [30]. It represents a use full tool for the virtual modelling of the new generations military special vehicles, with a focus on the drive system and on the suspension system, including magnetorheological damper, which has been experimentally tested [31];
- LS-DYNA to determine the value of dynamic forces acting on tank during overcoming selected terrain obstacles, by modelling and proper tuning the longitudinal and torsional characteristics of joints and rubber bushing [32];
- TRUCKSim for multibody dynamics combined with Matlab/Simulink to develop a real-time model for a driving simulator, in which 13 drivers assess the comfort of a passive and an active suspension of a tracked vehicle [33];
- AMESim to design a high-power density mechanical-electrical-hydraulic regenerative suspension system for tracked vehicles, improving endurance capacity, hence damping performance, without increasing energy consumption for active suspension [34];
- Dynamic Analysis Design System (DADS), LMS-CAE to simulate seismic signatures of moving armored vehicles: the methodology was applied on a M1 tank conducting simulations at constant and variable speed driving and cornering on high and low-friction surfaces [35].

Furthermore, the majority of experimental campaign carried out in the last year aimed at investigating the tracked vehicle suspension system and their influence on the dynamic response of the suspended mass. Regarding the first point, experimental outcomes have been used in Ref. [36] for the validation of a nonlinear hydro-gas suspension system, providing a soft spring rating at lower wheel travel and a hard spring rating at higher wheel travel. Meanwhile, an inverse problem technique, based on Particle Swarm Optimization (PSO) and on Random Restricted Window (R2W) is adopted for the estimation of suspension stiffness and damping coefficient of a tracked vehicle [37] with the aim of minimising the quadratic error between estimated and experimental data for bounce and pitch acceleration. A comparison between rigid and flexible road wheel arm models is presented in Ref. [38] to compute the response of the centre of gravity of the

vehicle, comparing it with experimental data, while a prototype of a tracked vehicle was developed in Ref. [39] to experimentally evaluate the torques on the drive shafts, the rotational speeds of the drive wheels and the dynamics of the vehicle suspended mass. The NVH performance are instead evaluated through noise and vibration measurements in a Viking military vehicle [40].

Due to the harsh conditions in which tracked vehicle are required to work [41], analyses on their components and sub-assemblies have been carried out. This is presented in Ref. [42] for fatigue crack detection on the crawler chain link of excavator and in Ref. [43] to understand the damage development in the elastomeric material, placed in the backerpad, namely in the region where road wheel repeatedly rolling over the pad. The testing conditions are not standardised as in automotive field, in which wheel manufacturers must satisfy strict safety requirements relying on specific experimental accelerated fatigue tests [44].

Finally, also the steering performance of tracked vehicles has been largely investigated in the last two decades. In this context, a theory for the skid steering of tracked vehicles under steady state conditions on firm ground, taking into account the shear stress—shear displacement relationship on the track—ground interface, was developed by Wong [45]. The novelty point consists in the introduction of a lateral friction coefficient, used to predict the moment of turning resistance, eliminating the necessity of experimental tests, as well. Instead, to reduce the computational effort, a transient steering model for tracked vehicles, implemented in Matlab/Simulink environment is developed in Ref. [46]. A nonlinear deformable terrain model [47] is introduced in the methodology proposed for lateral dynamics simulation of high-speed tracked vehicle, assessing adequate accuracy in predicting of steering performance, while a direct yaw torque control strategy is proposed in Ref. [48], through the use of four motors, to improve the output power of the outer driving wheels during steering, the running trajectory of the tracked vehicle, and its running stability. Furthermore, an analytical study of an articulated tracked vehicle is presented in Ref. [49], where a 8 DOFs mathematical model is developed to characterize the articulated steering behaviour that avoids any thrusts adjustment between the tracks, which is typical for skid-steering vehicles. Then, a hitch angle controller is also designed in Refs. [50,51], to control the cornering vehicle response by simulating typical maneuvers for handling analysis.

Recently, NVH issue of Ajax armoured vehicle [52] has emerged. The noise issue, "which causes also loss of hearing by crews trialling the platforms arose from the integration of the Bowman headsets for the crew radios, which were picking up engine noise, amplifying it as the vehicle accelerated, and putting the sound directly into the crews' ears". Surely, the engine is a critical source of NVH issues, since it can generate torsional vibrations in the transmission driveline, hence in the sprocket wheel which drives the track chain. Tracked vehicle are really complex systems, therefore their design must cover also all the possible dynamic aspects to avoid critical issues.

From the literature review analysis, it has emerged an interest in the development of mathematical and analytical models with few DOFs. These models, validated through experimental data or using multibody simulations, can predict the tracked vehicle ride dynamics with minimal computational costs. In this context, This paper aims to cover these aspects proposing the following points of novelty:

● the development of a full tracked vehicle model, starting from experimental characterisation of the track assembly system, in the customised FEM software LUPOS[53];
● the implementation of a Model Order Reduction (MOR), based on [54], to reduce the total number of DOFs of the

structure with a customised selection of the master DOFs and modal base, maintaining an accurate description of vehicle dynamic behaviour;
● the investigation of the track chain influence and speed variation, on the vertical dynamics of a tracked vehicle, both with frequency and time domain analyses.

The paper is organized as follows: Section 2 proposes the vehicle architecture and the concepts behind the vehicle modelling are illustrated. In Section 3, the MOR approach is presented and applied on the case study. Then, in Section 4, the simulation results in both time and frequency domains under several testing conditions are discussed. Finally, in Section 5, the outcomes of this research activity are drawn and possible future developments are proposed.

2. Vehicle architecture and modelling

In this paper, an armoured tracked vehicle has been considered for the study of its dynamic behaviour. Vehicle geometry has been estimated and its main dimensions are depicted in Fig. 1 (a). Starting from the available geometry, a modelling phase of different components, sub-assemblies and whole assembly has been conducted.

The first aim is the development of a simplified track chain model which well reproduce both static and dynamic properties. This is done by creating a Finite Element (FE) model of the single track assembly component, namely the ones composing the whole chain if connected each other. The FE model has been validated using the experimental characterisation of the mentioned component, as described in the following sections. Details of the considered tracked vehicle are reported in Figs. 1(b)−1(c). The analysed vehicle assembly can be subdivided in its main sub-assemblies:

● the sprung mass, *i.e* the hull: it is modelled as a rigid body with mass and inertial properties;
● the unsprung mass: the tracked vehicle counts 7 axles, therefore 14 road wheels, 7 for each track side,
● the suspension system: it is modelled with torsional bars, namely with a rod and a lever arm, which together connect the hull with the centre of unsprung masses;
● the track assembly, which will be described in details in the next sections, since it is the component on which the MOR is applied;
● the track chain, whose dimensions are estimated using Fig. 1 (a) and whose details are here specified:
   ○ the total number of track assembly components is 92, 30 of which in contact with the ground;
   ○ the total length of the chain is 14858 mm, with a length of the part touching the ground of 4845 mm;
   ○ the distance between the centre of two pins belonging to different track components is 65 mm: a rigid connection is assumed between these two pins.

Due to the purely academic purpose of this research, some of the sensible parameter values in Table 1 have been altered, while maintaining their value reasonable.

As already mentioned, one of the aim of this research activity is the investigation of vehicle vertical dynamics. Hence, the influence of the track chain and longitudinal vehicle speed have been assessed. Therefore, two different models of the vehicle have been created, as reported in Fig. 2. Besides the track chain, the two models are identical, since the sprung mass centre of mass is connected to one side of the suspension system by rigid connectors, *i.e.*, the black "spider structure" in Fig. 2. In the un-tracked vehicle only one track assembly has been modelled, while for the tracked
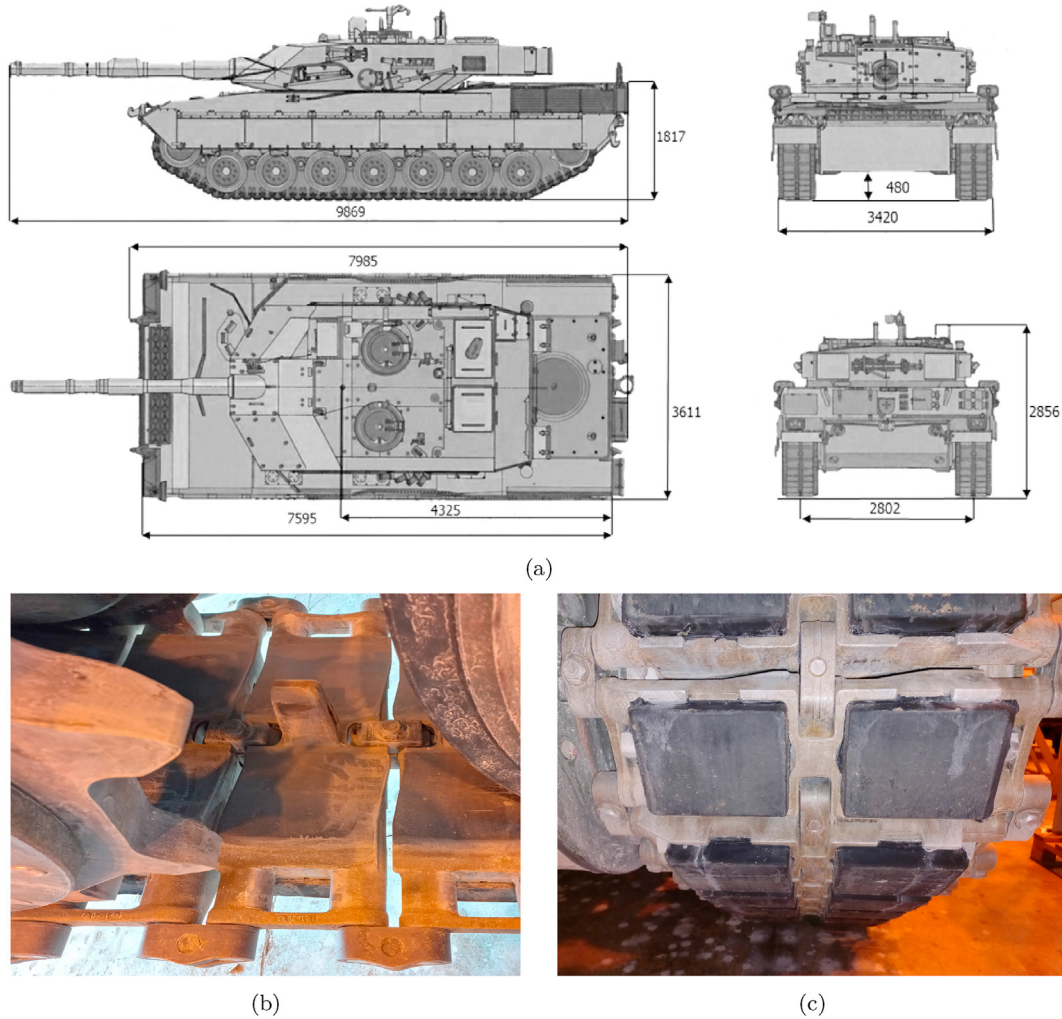
L. Dimauro, S. Venturini, A. Tota et al.

(a)

(b)

(c)

Fig. 1. Tracked vehicle (a) with details of tracks (b) and link pads (c).

Table 1
Vehicle parameters.

Type	Parameter	Value
Geometry	Length L	7.6 m
	Width B	3.42 m
	Height H	2.2 m
	Axle-to-Axle wheelbase l	0.78 m
	Track-to-Track width b	2.8 m
	Sprung mass CoG height h_G	1.57 m
Masses and inertia	Sprung mass m_s	30300 kg
	Roll moment of inertia I_x	$3.9 \cdot 10^4$ kg·m^2
	Pitch moment of inertia I_y	$1.4 \cdot 10^5$ kg·m^2
	Yaw moment of inertia I_z	$1.6 \cdot 10^5$ kg·m^2
	Unsprung mass m_u	$1.2 \cdot 10^3$ kg
	Track assembly mass m_t	27 kg
	Total mass m	$5.6 \cdot 10^4$ kg
Suspension	Torsional bar stiffness k_t	$5.2 \cdot 10^5$ N·m/rad
	Wheel vertical stiffness k_w	$2 \cdot 10^{10}$ N/m
Track assembly	Shear longitudinal stiffness k_x	$1.4 \cdot 10^6$ N/m
	Shear transversal stiffness k_y	$3.4 \cdot 10^6$ N/m
	Compression stiffness k_z	$18.95 \cdot 10^6$ N/m
	Torsional stiffness k_{ry}	$6.3 \cdot 10^4$ N·m/rad

vehicle the whole chain has been considered. In case of un-tracked vehicle, the centre of each road wheel is connected to one track assembly by a spring with a stiffness k_w. In LUPOS environment [53]

springs are marked by green lines. On the other hand, for the tracked vehicle, also the sprocket and the idle gears are connected to a certain number of track assemblies, as highlighted in Fig. 2 (b).

2.1. Track assembly

Main of the modelling efforts have been addressed on the design of the track assembly, which has been then experimentally tested to evaluate its mechanical properties.

2.1.1. CAD/CAE and FE model

As first step in the design process, the CAD model of the single track assembly component is created in SolidWorks using the geometrical dimensions of the real link, as depicted in Fig. 3. The generated track CAD model is made of 9 parts:

- 1 link, the main steel body of the track assembly on which the vehicle rests through the road wheels, *i.e.*, the unsprung masses;
- 2 rubber pads interacting with the terrain, which are inserted in two cavities of the link by interference. The two pads have a steel core of 3 mm;
- 2 steel pins interacting with the sprocket wheel, which transmit the power from the engine to pull the vehicle along the tracks. They are inserted across the whole length of the
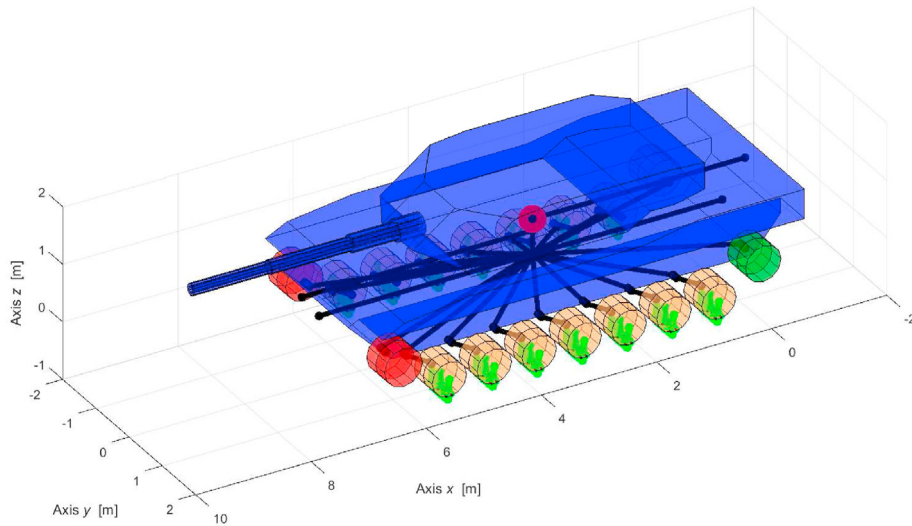
(a)
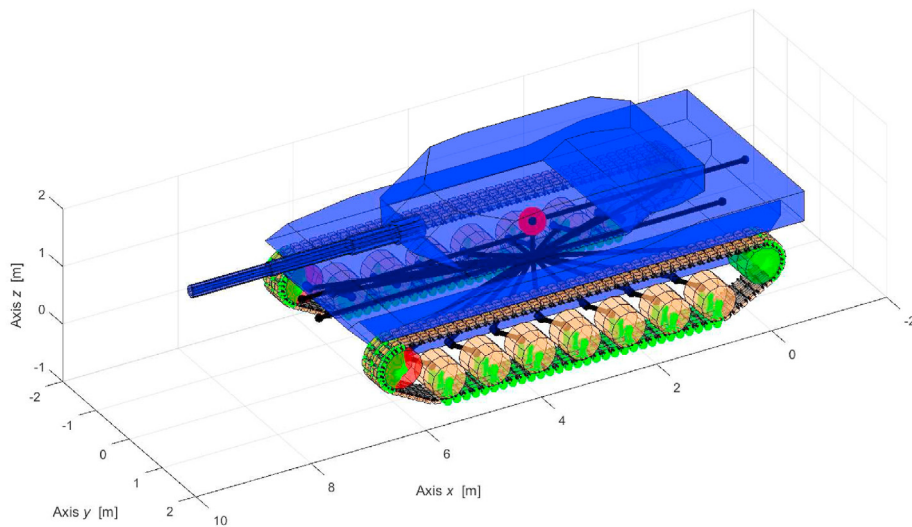
(b)

Fig. 2. Un-tracked (a) and tracked vehicle (b) models, developed in LUPOS environment.

link and are connected with the pins of the adjacent links through joints;

● 4 rubber O-rings, interposed between the link and the two pins.

2.1.2. Experimental material characterisation

The experimental activity was carried out with the Instron 8801 testing machine, reported in Fig. 4, which has been used to perform compression tests on the track assembly structure to evaluate the compression stiffness of the system and the material properties of pad rubber.

From experimental tests on Instron machine (Fig. 4) with a compression velocity of 40 mm/min a nonlinear stiffness of the track assembly has been evaluated, as reported in Fig. 5 (b). Analysing the load-stroke curve of the same test, depicted in Fig. 5 (a), a linear trend can be noted, hence it has been decided to consider a

linear fitted model, to have the smallest stiffness variation in the range 3.5–4.5 mm. Hence, the constant value k_z=18950 N/mm is computed for the whole track assembly stiffness. This value has been assumed to be the stiffness of the pad rubber, due the much higher stiffness of the link, made of steel material.

Experimental results are also used to assign the material properties in the SolidWorks model, to have the proper deformation of the pads under the same loading conditions. Hence, the material "AISI 1035 Steel" has been assigned to link, pins and steel plate inside the pad, while the material "SBR rubber" has been created for the pad rubber and for O-rings, to fulfill the experimental results, as listed in Table 2.

The rubber material has been tuned, through static FE analyses, to have a vertical compression of the upper surface of the track assembly of 1 mm, when a vertical load of 18950 N was applied to the track assembly, also reported in Fig. 6 (a). For the static analyses, a first order tetrahedral mesh is adopted with a characteristic size
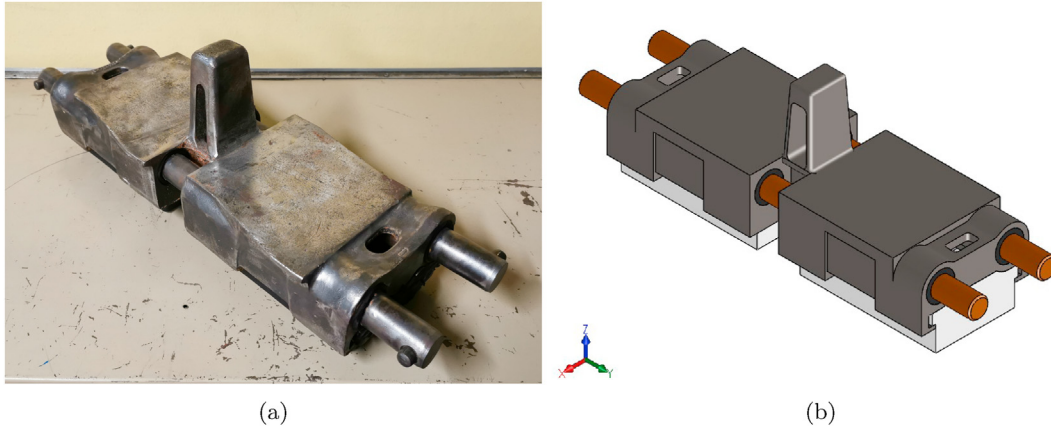
L. Dimauro, S. Venturini, A. Tota et al.

Fig. 3. Track assembly geometry: real component (a) and CAD model (b).
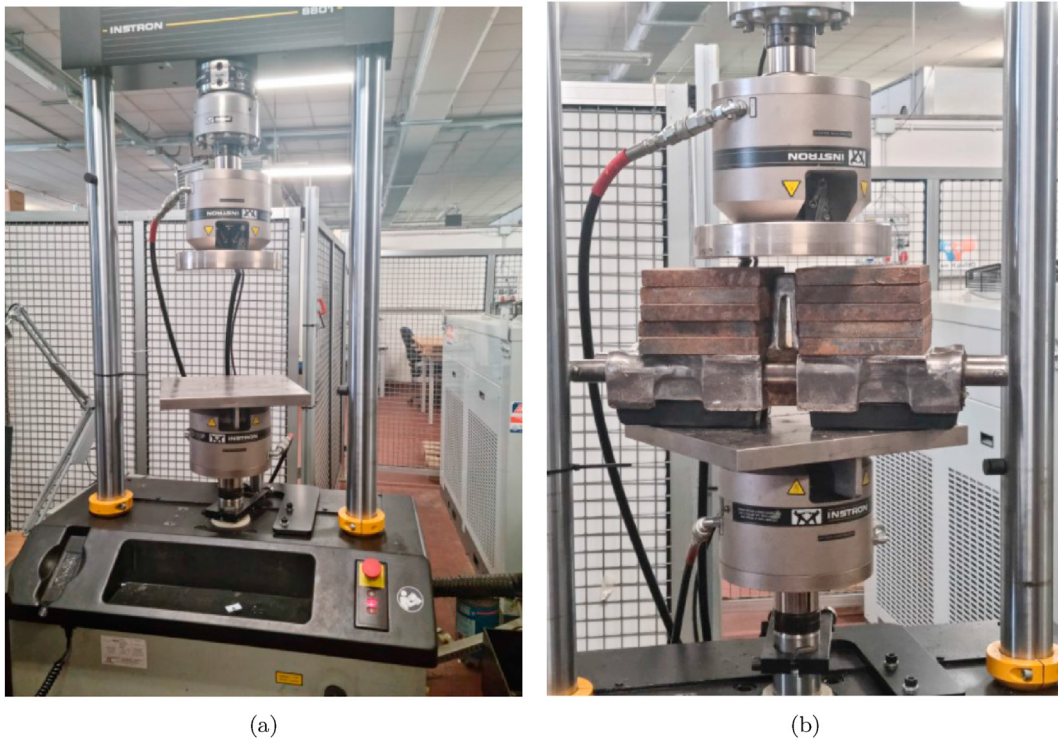

Fig. 4. Instron machine (a) for experimental characterisation of the track assembly component (b).

of 3 mm. The resulting number of nodes, elements and DOFs of the track assembly component is too high and any possible attempt in generating the whole chain model would be computationally too heavy. Therefore, it has been decided to progressively apply topological MOR.

2.1.3. LUPOS models: from 3D to 1D elements

The first proposed model has been created using 3D hexahedral elements, together with rod elements for the pins. The customised FEM software LUPOS [53], developed by the authors, has been used for the analyses proposed from now on. The resulting equivalent compression stiffness of the track assembly, *i.e.*, k_z, has been used to compute an equivalent Young modulus E_{pad} for the pad (in which the steel plate is not considered), by means of Eq. (1):

$$E_{pad} = \frac{k_z\, h}{A_{TOT}} = 25.84 \text{ MPa} \tag{1}$$

where A_{TOT} is the base surface of the track assembly given by the sum of the base surface of each pad, and h in the thickness of the rubber. For the first 3D model, Fig. 6 (b), the structure of the link has been simplified, removing the guide in the middle. Hexaedral elements are chosen for both link and pads, while the pins are modelled using 1D rod elements. The total number of DOFs of this 3D model (1638 for each track assembly) is still to high, to assembly the whole track chain. Therefore, the model has been further reduced, with the adoption of 1D elements and lumped springs. Indeed, for the second model (Fig. 6 (c)), made of only 1D elements, a set of 12 springs, arranged in series and in parallel in the pad of
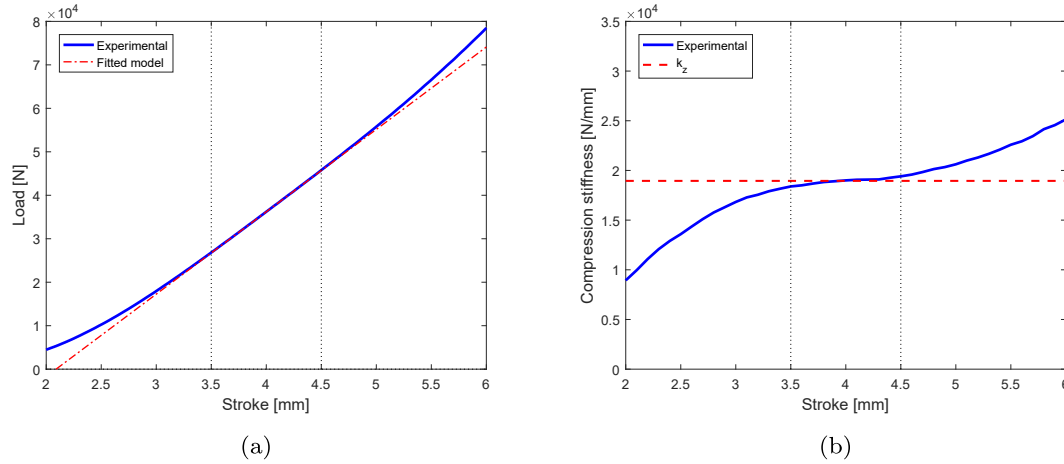
Fig. 5. Load-Stroke curve of the track assembly component (a) and its compression stiffness (b), experimentally tested using Instron machine with a velocity of 40 mm/min.

Table 2
Material properties in the SolidWorks track assembly model of Fig. 3 (b).

Material	Property	Value
AISI 1035 Steel	Young modulus E_{steel}	205 GPa
	Poisson ratio ν_{steel}	0.29
	Density ρ_{steel}	7850 kg/m^3
	Yield strength σ_{steel}	282.7 MPa
SBR rubber	Young modulus E_{pad}	9 MPa
	Poisson ratio ν_{pad}	0.48
	Density ρ_{pad}	1250 kg/m^3
	Yield strength σ_{pad}	2 MPa

Table 3
Progressive MOR in track assembly modelling: from 3D to 1D elements.

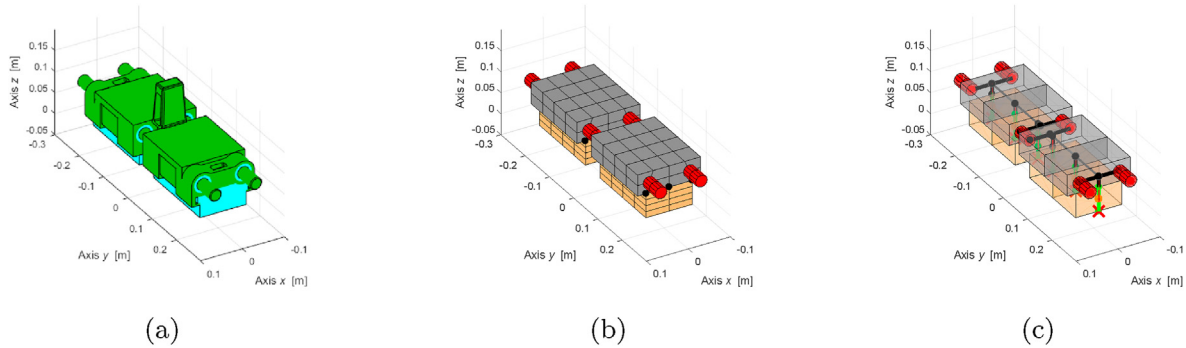| Model	3D SW	3D LUPOS	1D LUPOS
# of nodes	236305	318	44
# of 1D elements	–	12	88
# of hexahedral elements	–	128	0
# of tetrahedral elements	1285036	–	–
# of DOFs	1417830	1908	264
# of master-slave RJs	–	38	16
# of BCs	5135	42	36
# of active DOFs	1412695	1638	132

Fig. 6. Complexity reduction of the track assembly model: 3D SW (a), 3D LUPOS (b) and 1D LUPOS (c).

the track assembly, is adopted to have a global compression stiffness of the track assembly equal to the experimental one. As it is possible to see from this model, the nodes of the pad on the bottom surface have been constrained. Besides vertical stiffness in z direction, also shear longitudinal and transversal stiffness in x and y directions, respectively, and torsional stiffness along y axis are considered. Their values are computed from simulation on Solid-Works on the 3D model, with the right material properties. The model size has been reduced up to 132 DOFs for each track assembly, hence a feasible number to manage static simulations and to prepare dynamic simulations with the whole track chain, discussed in the next Subsection 2.2. A quantification of the progressive MOR in the track assembly modelling is reported in Table 3, with the reduced model having less than 0.01% of active nodes, if compared to the 3D model analysed in SolidWorks (SW).

2.1.4. Results of static analyses

The same load conditions have been applied to the three developed models, to verify the static deformation, due to a vertical load, acting on the upper surface of the link. Results are reported in Fig. 7, where two different views are proposed, to visualise both the vertical displacement and the displacements in the bottom surface, when hexahedral elements are adopted.

2.2. Track chain modelling

Therefore, the track chain has been modelled in LUPOS, using 1D elements, with two different level of details. As represented in Fig. 8 the connections between two adjacent track assemblies can be realised by means of rigid joints (RJs), *i.e.*, master-slave connections, or using real connectors allowing the rotation of the pin around Y

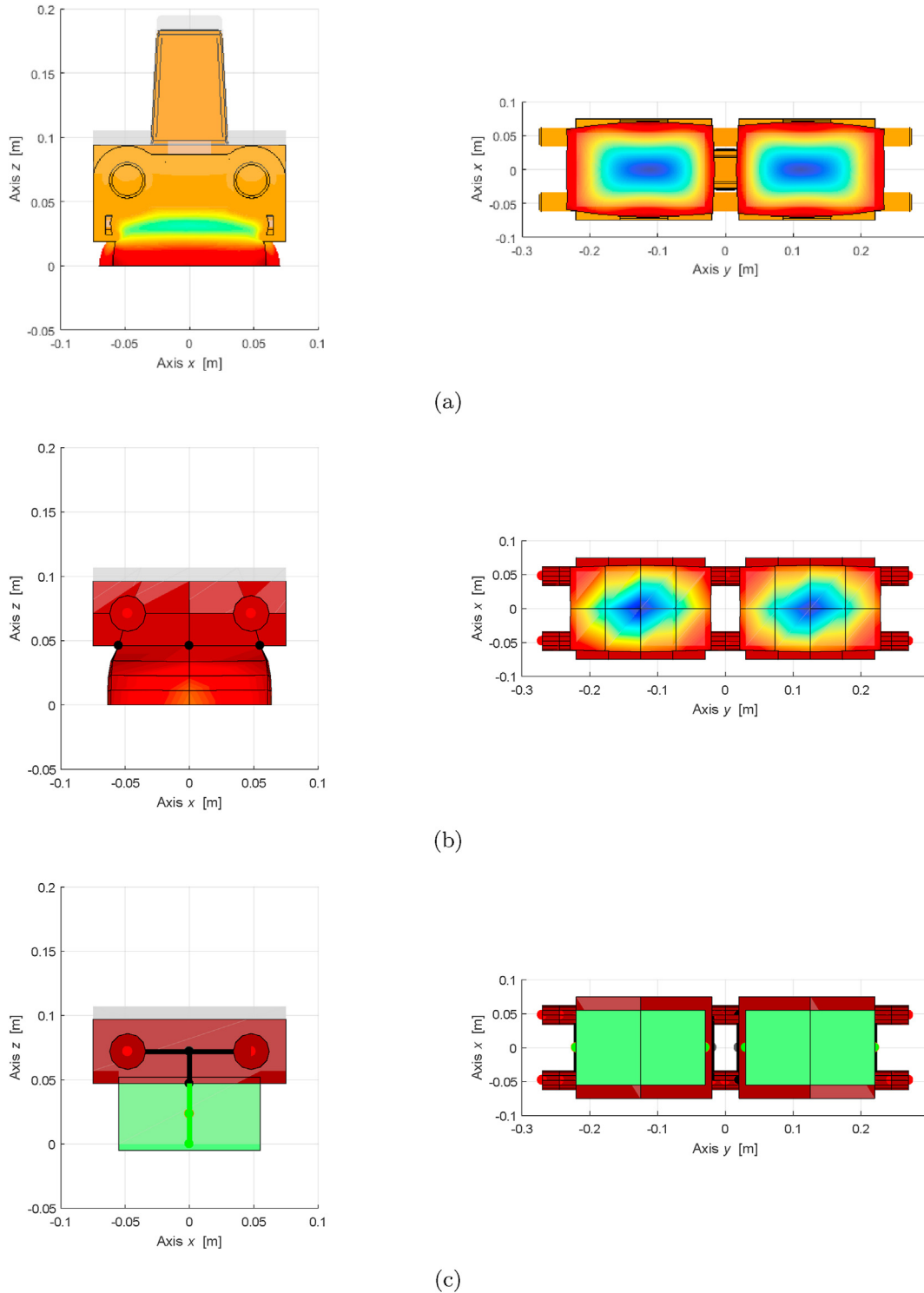*L. Dimauro, S. Venturini, A. Tota et al.*

Fig. 7. Static deformations in lateral (left) and bottom (right) views: 3D SW (a), 3D LUPOS (b), 1D LUPOS (c) models.

axis. In this last case, an additional torsional stiffness, corresponding to the stiffness between steel pins and connecting elements should be add in the model. For sake of simplicity, and for the absence of experimental data to proper tune this parameter, the authors have decided to adopt the configuration with rigid joints (RJs), for what presented in the next sections.

3. Model order reduction

The depicted final models developed in previous Section 2, describe the vehicle dynamic behaviour with a large amount of DOFs. The number of DOFs affects the dimensions of model matrices with a strong impact on computational costs. The topological MOR introduced at the track assembly component is a
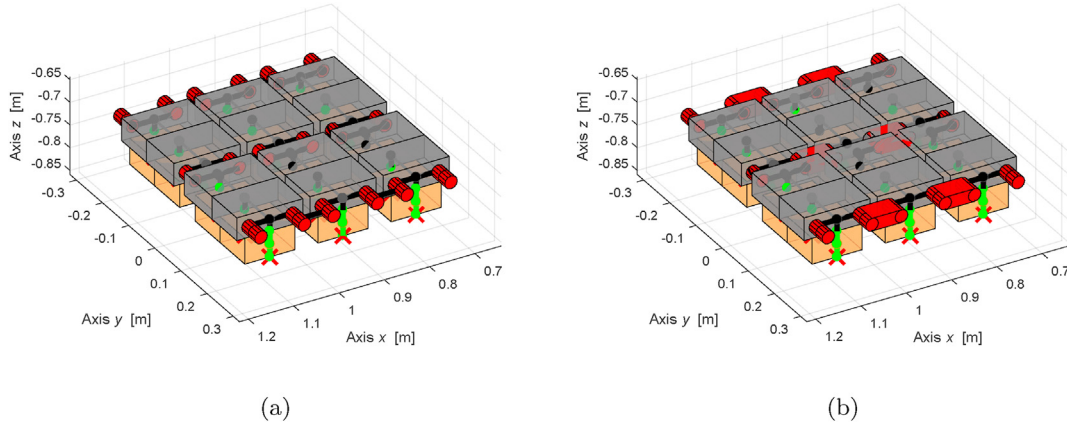
Fig. 8. LUPOS model of a sequence of 3 track components using RJs (a) or real connection (b).

significant step in reducing simulation times. Nevertheless, the simulated vehicle still globally presents 184 track assemblies which are the most significant contribution to model complexity.

3.1. Component Mode Synthesis

Component Mode Synthesis (CMS), a well known MOR technique for dynamic analyses [54], is adopted to reduce the number the total number of DOFs of the structure while retaining accurate description of its dynamic behaviour. The whole vehicle, i.e., the assembly made of chassis, suspensions, wheels and track chains, is considered as a substructure interacting with the ground through track pad equivalent springs.

The linear time invariant system of Eq. (2) with n active DOFs is given:

$$\mathbf{M}\ddot{\mathbf{x}} + \mathbf{C}\dot{\mathbf{x}} + \mathbf{K}\mathbf{x} = \mathbf{f} \tag{2}$$

where:

- $\mathbf{x}$, $\dot{\mathbf{x}}$, and $\ddot{\mathbf{x}}$ are the generalised displacements, velocities and accelerations ($n{\times}1$), respectively, of the active DOFs;
- $\mathbf{M}$ is the mass matrix ($n{\times}n$), real, symmetric, positive definite, to confirm only positive inertial properties;
- $\mathbf{C}$ is the damping matrix ($n{\times}n$), real, symmetric, positive semi-definite or definite to allow distributed or localised energetic dissipation;
- $\mathbf{K}$ is the stiffness matrix ($n{\times}n$), real, symmetric, positive semi-definite to include also some rigid body motions, or positive definite to allow only elastic deformations;
- $\mathbf{f}$ is the generalised force vector ($n{\times}1$) acting on active DOFs, real.

The $\mathbf{K}$ matrix and $\mathbf{x}$ vector can be partitioned, by reordering substructure DOFs in master m and subordinate s ones:

$$\begin{Bmatrix} \mathbf{f}_m \\ \mathbf{f}_s \end{Bmatrix} = \begin{bmatrix} \mathbf{K}_{mm} & \mathbf{K}_{ms} \\ \mathbf{K}_{sm} & \mathbf{K}_{ss} \end{bmatrix} \begin{Bmatrix} \mathbf{x}_m \\ \mathbf{x}_s \end{Bmatrix} \tag{3}$$

Master DOFs represent the interface of the substructure with the external environment, while subordinate DOFs are internal the substructure and may interact with m and/or other s DOFs. Therefore, the partition in Eq. (3) emphasises the coupling between the loads $\mathbf{f}_m$, $\mathbf{f}_s$ and displacements $\mathbf{x}_m$, $\mathbf{x}_s$ through stiffness matrix K partitions.

Supposing the subordinate internal loads $\mathbf{f}_s = \mathbf{0}$, i.e., the substructure is excited only externally, the subordinate internal displacements $\mathbf{x}_s$ depend only from the stiffness partitions and the master displacements $\mathbf{x}_m$.

$$\mathbf{x}_s = -\mathbf{K}_{ss}^{-1}\mathbf{K}_{sm}\mathbf{x}_m = \mathbf{\Phi}_C\mathbf{x}_m \tag{4}$$

The product term of stiffness partitions $\mathbf{K}_{ss}$, $\mathbf{K}_{ss}$ in Eq. (4) represents the $\mathbf{\Phi}_C$ constraint modes of the system based on the boundary condition unitary displacements. Constraint modes $\mathbf{\Phi}_C$ can be used to express the subordinate internal displacements $\mathbf{x}_s$ as a function of interface displacements $\mathbf{x}_m$.

$$\mathbf{f}_m = [\mathbf{K}_{mm} + \mathbf{K}_{ms}\mathbf{\Phi}_C]\mathbf{x}_m \tag{5}$$

The undamped substructure with the selected m master DOFs, has an internal dynamics which depends on $\mathbf{M}_{ss}$ and $\mathbf{K}_{ss}$ only. Hence, eigenfrequencies ω_i and eigenvectors $\mathbf{\Phi}_{S,i}$, i.e., constrained substructure flexible modes, can be obtained by solving the corresponding eigenproblem and using the following equality:

$$\omega_i^2\mathbf{M}_{ss}\mathbf{\Phi}_{S,i} = \mathbf{K}_{ss}\mathbf{\Phi}_{S,i} \tag{6}$$

Internal substructure $\mathbf{\Phi}_S$ flexible modes are collected:

$$\mathbf{\Phi}_S = [\mathbf{\Phi}_{S,1}, ..., \mathbf{\Phi}_{S,1}, ...\mathbf{\Phi}_{S,r}] \tag{7}$$

And the transformation matrix $\mathbf{T}_{CMS}$ is composed:

$$\mathbf{T}_{CMS} = \begin{bmatrix} \mathbf{I} & \mathbf{0} \\ \mathbf{\Phi}_C & \mathbf{\Phi}_S \end{bmatrix}_{((m+s)\times(m+r))} \tag{8}$$

$\mathbf{T}_{CMS}$ is a rectangular reduction matrix, where the reduction occurs through:

- the significant selection of master DOFs, i.e., the minimisation of m;
- the significant selection of $\mathbf{\Phi}_S$ flexible modes, i.e., the minimisation of r.

In case of proportional damping, the reduction is applied to all the substructure matrices:

$$\begin{aligned} \mathbf{M}_R &= \mathbf{T}_{CMS}^{\mathrm{T}} \, \mathbf{M} \, \mathbf{T}_{CMS} \\ \mathbf{C}_R &= \mathbf{T}_{CMS}^{\mathrm{T}} \, \mathbf{C} \, \mathbf{T}_{CMS} \\ \mathbf{K}_R &= \mathbf{T}_{CMS}^{\mathrm{T}} \, \mathbf{K} \, \mathbf{T}_{CMS} \end{aligned} \tag{9}$$

Finally, the reduced description of the substructure dynamic behaviour occurs through $\mathbf{x}_R = \{\mathbf{x}_m \ \mathbf{x}_r\}^{\mathrm{T}}$ where $\mathbf{x}_r$ are non-physical

displacements related to flexible modes.

$$\mathbf{M}_R \ddot{\mathbf{x}}_R + \mathbf{C}_R \dot{\mathbf{x}}_R + \mathbf{K}_R \mathbf{x}_R = \mathbf{f}_R \qquad (10)$$

The proper selection of $\mathbf{\Phi}_S$ with respect to the required bandwidth of application of the model, and interface DOFs against the loading conditions, allows to reduce the dimension of the substructure matrices, therefore the computational cost.

In the next subsections, the flexible mode selection and the interface DOFs definition will be performed.

3.1.1. Mode selection

The flexible mode selection is performed by using Modal Assurance Criterion (MAC) [55] to identify tracked vehicle model mode shapes, significant for the global vehicle dynamic behaviour.

The function of the MAC is to provide a measure of the correlation between two real eigenvectors $\mathbf{\Phi}_j$ and $\mathbf{\Phi}_k$. The MAC definition is:

$$MAC_{j,k} = \frac{\left[\mathbf{\Phi}_j^{\mathsf{T}} \mathbf{\Phi}_k\right]^2}{\left[\mathbf{\Phi}_j^{\mathsf{T}} \mathbf{\Phi}_j\right]\left[\mathbf{\Phi}_k^{\mathsf{T}} \mathbf{\Phi}_k\right]} \qquad (11)$$

when $\mathbf{\Phi}_j$ and $\mathbf{\Phi}_k$ are identical mode shapes, the MAC is equal to 1, while completely different mode shapes give MAC equal to 0.

In this application, the MAC is applied on two different configurations of the tracked vehicle model, *i.e.*, the minimal track chain uncoupled one and the completely coupled one. Moreover, the analysis is limited to the first 40 modes of both models, limiting the MOR to the identification of global vehicle mode shapes to 0−30 Hz bandwidth of interest for vertical vehicle dynamics. Obviously, the MAC application is limited to the common DOFs in both models. Also, rotational DOFs are ignored, by preferring equivalent translation DOFs.

Fig. 9 shows the MAC applied to the defined mode shape groups. On the abscissa, are present the modes of the tracked vehicle model with minimal track chain, while on the ordinates the modes of the fully tracked one. At each location, the MAC has been coloured with two different colour schemes: in gray scale the mode correlation under 70%, hence less significant, while in red scale the mode correlation over 70%. In Fig. 9, the correlation among mode #20 has been ignored since outside bandwidth of interest and also low
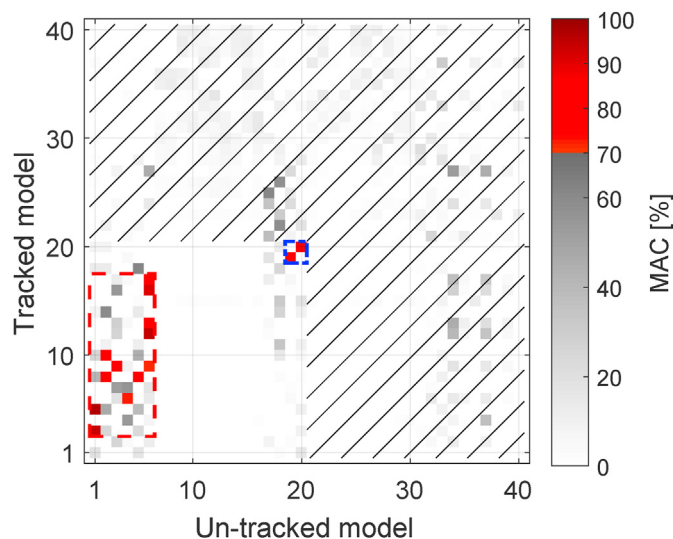
MAC. The MAC is generally low since the track chain presence in the model introduces many new track chain local modes which are not representative of global vehicle dynamics. This MAC application allows to use the more complex tracked vehicle model to filter discern the vehicle global modes which are present also in the minimal track chain model. Indeed, few high MAC combinations have been marked with red and blue dashed squares in Fig. 9: the red region contains sprung mass global vehicle modes, while the blue one unsprung mass global vehicle modes.

Fig. 10 shows the mode selection for the CMS application on both models. The graph is limited to Fig. 9 modes in which the MAC≥70%; *i.e.*, the red ones. Moreover, the black dashed curve represents the iso-frequency condition between the two models. If a MAC marker is on the iso-frequency curve, that mode is present in both models at the same eigenfrequency. Fig. 10 shows how the track chain model has globally higher natural frequencies than the minimal track chain one. This condition depends more on the additional track chain stiffness than the additional mass. Moreover, the contemporary high MAC of more fully track chain model modes with a single one of the minimal track chain model is related to the track chain coupling dynamics present in more mode shapes.

Table 4 shows the correlation list between the two models. The f_{UV} symbol refers to un-tracked vehicle model, while f_{TV} to the tracked one. Eventually, the correlation list presents curly bracketed values when the MAC is not maximum. The correlation list depicts the first 6 modes of sprung mass related to rigid translational and rotational behaviours. The longitudinal and lateral behaviours are coupled to pitch and roll since non-symmetric centre of gravity position and uneven distribution of contact stiffness to ground.

The effect of fully track chain coupling on the eigenfrequencies it to almost double the sprung mass bandwidth from 2.60−6.73 Hz to 5.25−13.7 Hz and an increase of about 60%−70% of unsprung mass eigenfrequencies.

Fig. 11 shows the detailed comparison between minimal track chain coupling and tracked model mode shapes. The comparison is performed in case of highest MAC (see Fig. 10). In the figure, the colour map is red for highest modal displacement, while is blue for null modal displacement. Moreover, the sprung mass barycentre is depicted by a large red round marker. Figs. 11(a)−11(f) refer to sprung mass mode shapes: the correspondence is high and the
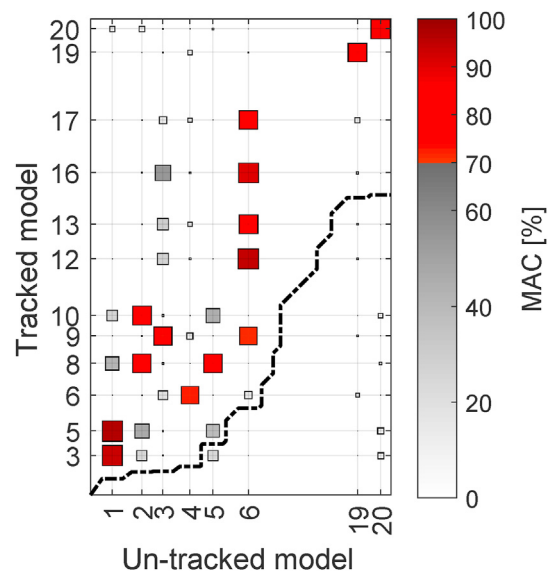

Fig. 9. MAC index applied to vehicle model mode shapes.

Fig. 10. Mode selection based on MAC index.

a) Mixed longitudinal and pitch behaviour (MAC=96 %).

b) Pitch behaviour around vehicle barycentre (MAC=81 %).

c) Mixed lateral and roll behaviour (MAC=74 %).
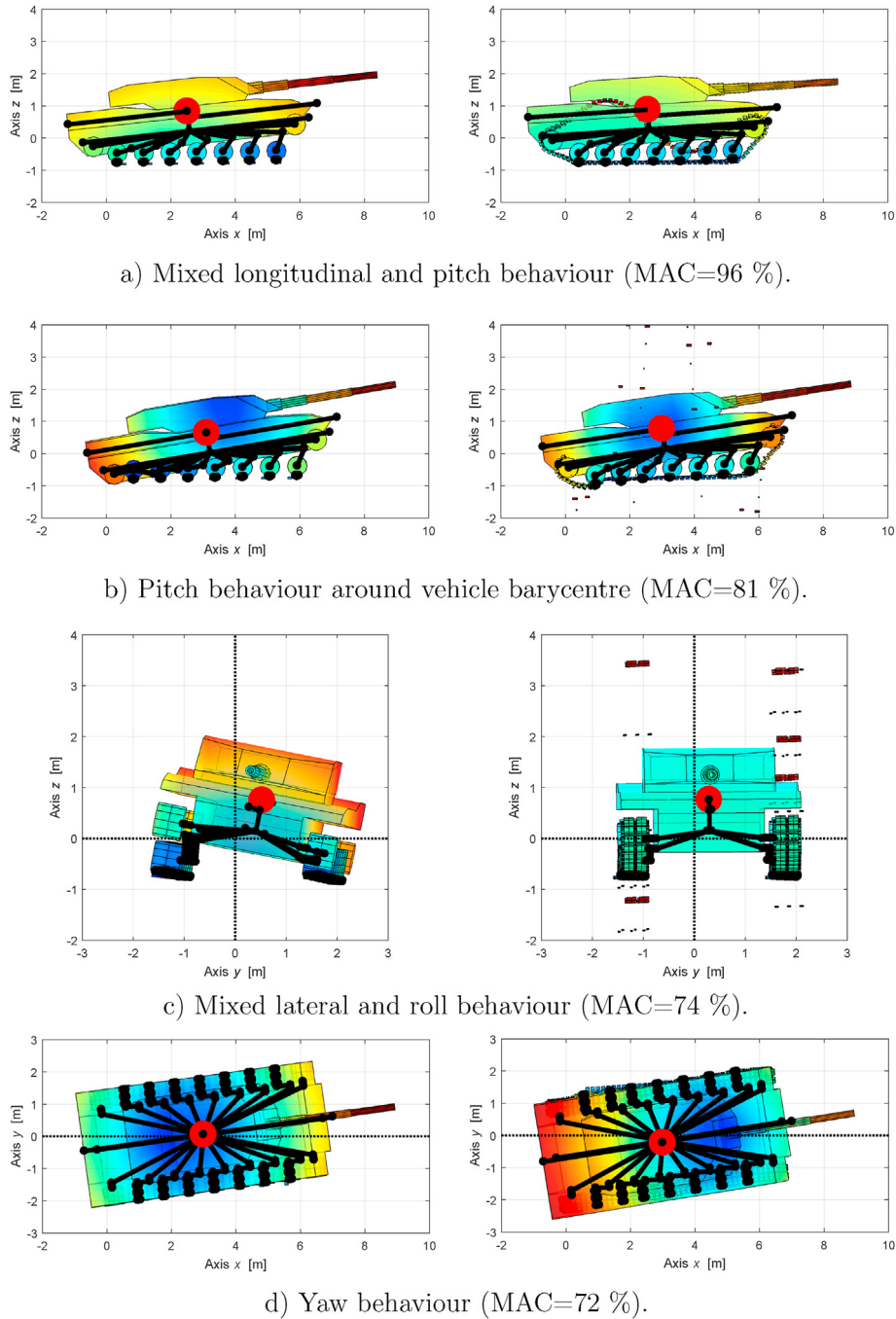

d) Yaw behaviour (MAC=72 %).

Fig. 11. Vehicle model mode shape comparison: minimal track chain coupling (left) and tracked model (right): Please, insert letters (a), (b), etc after the subfigure labels, as corrected for all the other figures.

slight contribution is given by the track chain modal displacement. In Fig. 11(a) case, the upper track chain sections show second flexural mode, while in Fig. 11(e) case, the third flexural mode occurs. Instead, Figs. 11(g)−11(h) show unsprung mass modes which are marginally related to roll and pitch of sprung mass. In Fig. 11(g) case, the left and right are out-of-phase, the sprung mass rolls to maintain the overall vehicle centre of gravity unaltered. Similarly, in Fig. 11(h) case the left and right are in-phase, hence the sprung mass pitches.

Summarising, a set of 8 flexible modes is selected for the minimal track chain coupled model and 12 flexible modes for the fully track chain coupled one.

### 3.1.2. Interface degrees of freedom

In this subsection, the fixed interface DOFs are selected using the Modal Geometric Selection Criterion (MoGeSeC) [56], an optimal criterion to select the most significant DOFs depicting the modal behaviour of a structure. The method can be used for optimal sensor placement in structural dynamics, and for MOR as in this application.

At each progressive iteration, the methodology computes the weight **W** for all **x** DOFs of the structure, and identifies the q DOF with highest W to be a master DOF. The method is interrupted when a prescribed number of master DOFs is reached and can start from an imposed initial condition with defined master DOFs.
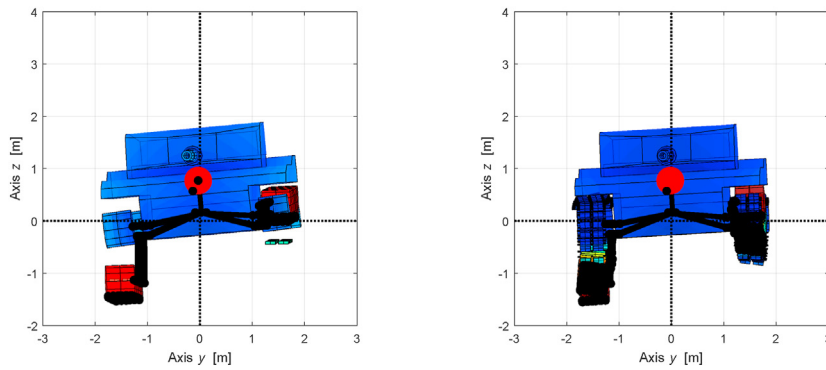
The weight **W** is computed as an element-wise product of the normalised modal weight $\mathbf{W}_{\Phi,N}$ and the normalised geometrical weight $\mathbf{W}_{g,N}$.
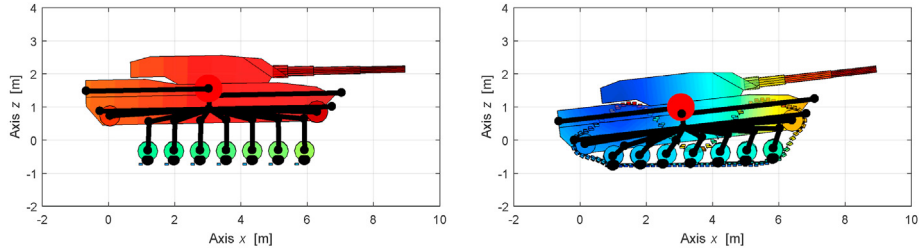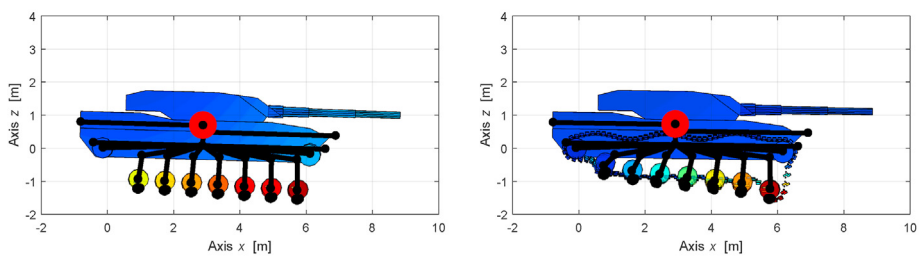

e) Bounce behaviour: out-of-phase
sprung and unsprung masses (MAC=80 %).
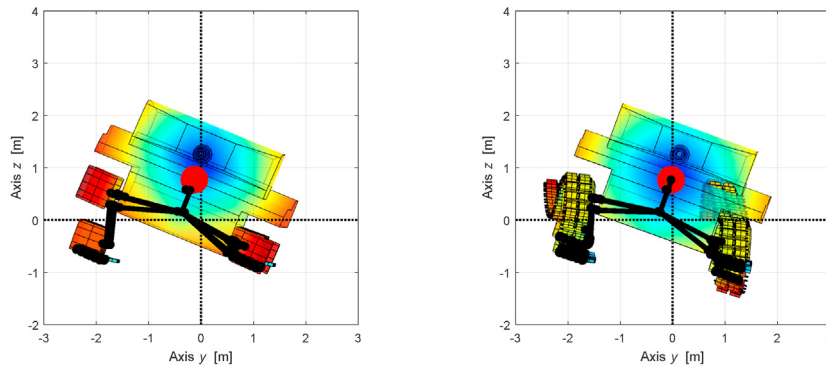
f) Roll sprung mass behaviour its barycentre (MAC=94 %).

g) Mixed roll and wheel bounce behaviour:
out-of-phase left and right axles (MAC=81 %).

h) Mixed pitch and wheel bounce behaviour:
in-phase left and right axles (MAC=86 %).

Fig. 11. (*continued*).

Table 4
Vehicle model eigenfrequency correspondence list: 0–30 Hz bandwidth.

Φ_{UV}	f_{UV} /Hz	Φ_{TV}	f_{TV} /Hz	Type
1	2.60	(3) 5	(4.73) 5.25	Longitudinal+Pitch
2	3.72	(8) 10	(8.49) 9.37	Pitch
3	3.79	9	9.36	Lateral+Roll
4	4.61	6	7.12	Yaw
5	4.93	8	8.49	Bounce
6	6.73	(9) 12 (13) (16) (17)	(9.36) 13.7 (15.5) (19.2) (23.1)	Roll
19	17.4	19	28.77	Wheel bounce+Roll
20	17.7	20	29.1	Wheel bounce+Pitch

$$\mathbf{W} = \mathbf{W}_{\Phi,N}\mathbf{W}_{g,N} = \frac{\mathbf{W}_\Phi}{\max(\mathbf{W}_\Phi)} \frac{\mathbf{W}_g}{\max(\mathbf{W}_g)} \tag{12}$$

$\mathbf{W}_{\Phi,N}$ and $\mathbf{W}_{g,N}$ are normalised with the maximum value at each iteration, in such a way the maximum of normalised weights is unitary, hence the overall weight W. For each DOF q, the modal weight $W_\Phi(q)$ is computed once at the beginning of the methodology and is a powered sum of q modal displacements in the mode set of n_Φ modes. The exponent $k_\Phi = 2$ is optimised in Ref. [56] for best identification.

$$W_\Phi(q) = \sum_{j=1}^{n_\Phi} \left| \mathbf{\Phi}_j^{(q)} \right|^{k_\Phi} \tag{13}$$

Instead, the geometrical weight $W_g(q)$ is computed at each iteration, and depends on the number n of master DOFs already identified. The p coefficient defines the order of the norm, which in this application is Euclidean, *i.e.*, $p = 2$. k_g is the power coefficient used to optimised the contribution of geometrical weight, usually $k_g = 2$ [56]. In $n > 0$ case, the geometrical weight is higher for DOFs which are far from already picked ones, inducing the spread of master DOFs.

$$W_g(\mathbf{q}) = \begin{cases} 1 & \text{if } n = 0 \\ 1 / \sum_{i=1}^{n} \left(\mathbf{q} - \mathbf{q}_i^{\,p} \right)^{-k_g p} & \text{otherwise} \end{cases} \tag{14}$$

The method is applied on the two models imposing input DOFs at centre of the wheels and the sprung mass DOFs as initial master DOFs, while the input mode sets have been identified in Subsection 3.1.1.

Fig. 12 shows the graphical result of the identification of the first 10 master DOFs for the two models. The red markers identify the initial master DOFs, identical for both models, while the other coloured markers refer to additional DOFs. The circular markers refer to vertical displacement DOFs, while triangular ones to lateral displacement. The methodology identifies other master DOFs on the encumbrance of the vehicle, preferring vertical DOFs to lateral ones. Moreover, in the tracked vehicle model case, also track chain DOFs are considered to distinguish the mode packages (see Table 4: modes 1, 2, and 6).

3.2. Model complexity comparison

In this subsection, the CMS method is applied and the complexity of original models and reduced ones is compared.

Table 5 shows the characteristics of the two models and the level of reduction reached. Thanks to the CMS approach and the selection with MAC and MoGeSeC, the reduced models are 5.6% and 2.4% of the size of the original corresponding tracked vehicle models.

4. Vehicle dynamic response

In this section, the un-tracked and tracked vehicle model responses are investigated and compared in frequency and time domains. The investigation in frequency domain is used to validate the MOR mode truncation and the track chain coupling effect on the unsprung mass frequency response. Also, the time domain analysis is used to validate the assumed bandwidth of interest for vertical tracked vehicle dynamics, and the track chain coupling

Table 5
MOR applied on developed tracked models.

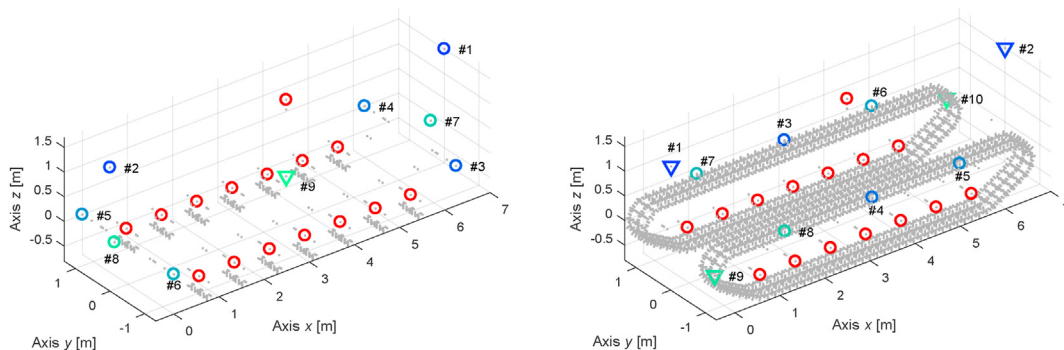| Model	Minimal tracked vehicle	Fully tracked vehicle
Active DOFs	2192	16856
Interface DOFs	84	360
Input DOFs	21	21
MoGeSeC DOFs	9	9
Flexible modes	8	12
CMS DOFs	122	402
Reduced size	5.6%	2.4%

Fig. 12. Significant master DOFs identified by MoGeSeC: un-tracked (left) and tracked (right) vehicle models.

effect on sprung mass vertical dynamics. Several tracks are considered in the analysis.

4.1. Comfort frequency response functions

In frequency domain, the vertical behaviour, *i.e.* comfort, is analysed mimicking the automotive field using acceleration frequency response functions (FRF) against vertical profile of sprung and unsprung masses.

The most important acceleration FRFs in vehicle comfort study are:

- sprung mass vertical acceleration FRF, *i.e.*, $\frac{\ddot{z}_s}{h}(\omega)$
- sprung mass pitch angular acceleration FRF, *i.e.*, $\frac{\ddot{\theta}_s}{h}(\omega)$
- front unsprung mass vertical acceleration FRF, *i.e.*, $\frac{\ddot{z}_{uF}}{h}(\omega)$
- rear unsprung mass vertical acceleration FRF, *i.e.*, $\frac{\ddot{z}_{uR}}{h}(\omega)$

By considering the system equations of motion in matrix form, the vertical harmonic excitation is obtained by an imposed vertical road profile law **u** and **u̇** in displacement and speed.

$$\mathbf{M}\,\ddot{\mathbf{x}} + \mathbf{C}\,\dot{\mathbf{x}} + \mathbf{K}\,\mathbf{x} = \mathbf{C}_u\dot{\mathbf{u}} + \mathbf{K}_u\mathbf{u} \tag{15}$$

The right-hand side excitation to the system occurs through the unsprung mass stiffness and damping to the ground $\mathbf{K}_u$ and $\mathbf{C}_u$. The harmonic generalised displacements and vertical road profiles can be expressed in Euler notation.

$$\begin{aligned}\mathbf{x} &= \mathbf{x}_0 e^{j\omega t}\\ \mathbf{u} &= \mathbf{u}_0 e^{j\omega t}\end{aligned} \tag{16}$$

where ω is the operative frequency which is related to the longitudinal vehicle speed v and the characteristic length of the harmonic road profile λ.

$$\omega = 2\pi\frac{v}{\lambda} \tag{17}$$

The generalised acceleration modulus vector $\ddot{\mathbf{x}}_0(\omega)$ can be obtained by substituting Eq. (16) in Eq. (15).

$$\ddot{\mathbf{x}}_0(\omega) = -\omega^2\left(-\omega^2\mathbf{M} + j\omega\,\mathbf{C} + \mathbf{K}\right)^{-1}(j\omega\,\mathbf{C}_u + \mathbf{K}_u)\,\mathbf{u}_0 \tag{18}$$

Eq. (18) is computationally expensive even using CMS reduced model in Eq. (10), since requires the inversion of the dynamic stiffness term. Since the dynamic stiffness inverse is the receptance matrix $\alpha(\omega)$, Eq. (18) can be rewritten as:

$$\ddot{\mathbf{x}}_0(\omega) = -\omega^2\alpha(\omega)(j\omega\,\mathbf{C}_u + \mathbf{K}_u)\,\mathbf{u}_0 \tag{19}$$

where it is not necessary to compute the whole $\ddot{\mathbf{x}}_0(\omega)$ since only few evaluations are necessary to study comfort. The receptance matrix are easily computed by Eq. (20):

$$\alpha_{jk}(\omega) = \frac{x_j}{F_k} = \sum_{r=1}^{n}\frac{\varphi_{jr}\varphi_{kr}}{\omega_r^2 + j2\zeta_r\omega_r\omega - \omega^2} \tag{20}$$

where ω_r and $\mathbf{\Phi}_r$ are eigenfrequency and eigenvector of the r-th mode, and ζ_r is the r-th modal damping factor obtained by modal analysis and modal coordinates decomposition.

In order to compute FRFs, the road profile amplitude can be expressed as the product of a fundamental harmonics h for a delay vector τ.

$$\mathbf{u}_0 = \tau\,h \tag{21}$$

The delay vector τ is unitary if a synchronous excitation of the system at input DOFs occurs.

$$\tau = \{\,1 \quad \cdots \quad 1\,\}^{\mathsf{T}} \tag{22}$$

Instead, τ is a complex vector when the road profile is travelled at a the longitudinal vehicle speed v.

$$\tau = \{\,e^{-j\omega\tau}(q_1) \quad \cdots \quad e^{-j\omega\tau}(q_n)\,\}^{\mathsf{T}} \tag{23}$$

In this case, the delay τ_q at each input DOF depends on its longitudinal location L_q with respect to v.

$$\tau_q = \frac{L_q}{v} \tag{24}$$

Therefore, the generalised acceleration FRF expression becomes

$$\frac{\ddot{q}_j}{h}(\omega) = -\omega^2\alpha_j(\omega)(j\omega\mathbf{C}_u + \mathbf{K}_u)\tau \tag{25}$$

where $\alpha_j(\omega)$ represents all the receptance terms for the j-th output.

4.1.1. Model order reduction approximation

The effectiveness of MOR, proposed in 3.1, is here investigated. The vertical acceleration and the pitch angular acceleration of the sprung mass over the road input, $\frac{\ddot{z}_s}{h}(\omega)$ and $\frac{\ddot{\theta}_s}{h}(\omega)$, are reported in Fig. 13.

In Fig. 13 (a) it is shown the comparison between the un-tracked vehicle model sprung mass FRFs and the corresponding CMS reduced model in the 0−50 Hz bandwidth. By recalling Subsection 3.1, the modal truncation was performed in 0−30 Hz, hence the two FRFs are consistent up to the threshold of 30 Hz, indicated by a vertical dash-dot black line, in correctly depicting the frequency content necessary to describe the un-tracked vehicle comfort behaviour.

Similarly, Fig. 13 (b) shows the comparison of sprung mass FRFs for the tracked vehicle models. There is a resonance frequency almost coincident with the truncation threshold. Nevertheless, the latter is well reproduced by the CMS model in amplitude while a 2% of error occurs in resonance frequency.

From now on, since the un-tracked and tracked CMS models have been validated in frequency domain, they will be exclusively used in this section.

4.1.2. Track coupling effect

The most significant effects of the presence of the track in the vehicle is the coupling in the vehicle comfort dynamics and the stiffening of the vehicle suspension system. Although the track chain introduction lead to an increment of the global system mass, suggesting a reasonable reduction in frequencies, the consequently stiffness effect, due to the rigid connections between the track assemblies has a greater effect. In Fig. 14, it is shown the comparison of un-tracked vehicle (UV) and tracked vehicle (TV) sprung mass FRFs. The TV resonance frequencies are higher since additional stiffness given by the track.

The red arrows show the frequency transition of sprung mass resonance frequencies, while the blue arrow is related to the unsprung mass bouncing, coupled with the sprung mass pitch. Differently from automotive field, where the suspension dynamics is an order of magnitude higher in frequency than the sprung mass, in this tracked vehicle the ratio is about 3.

4.1.3. Wheelbase filter

In this section, the effect of different road profile harmonic content is shown on the comfort FRFs. In fact, while synchronous
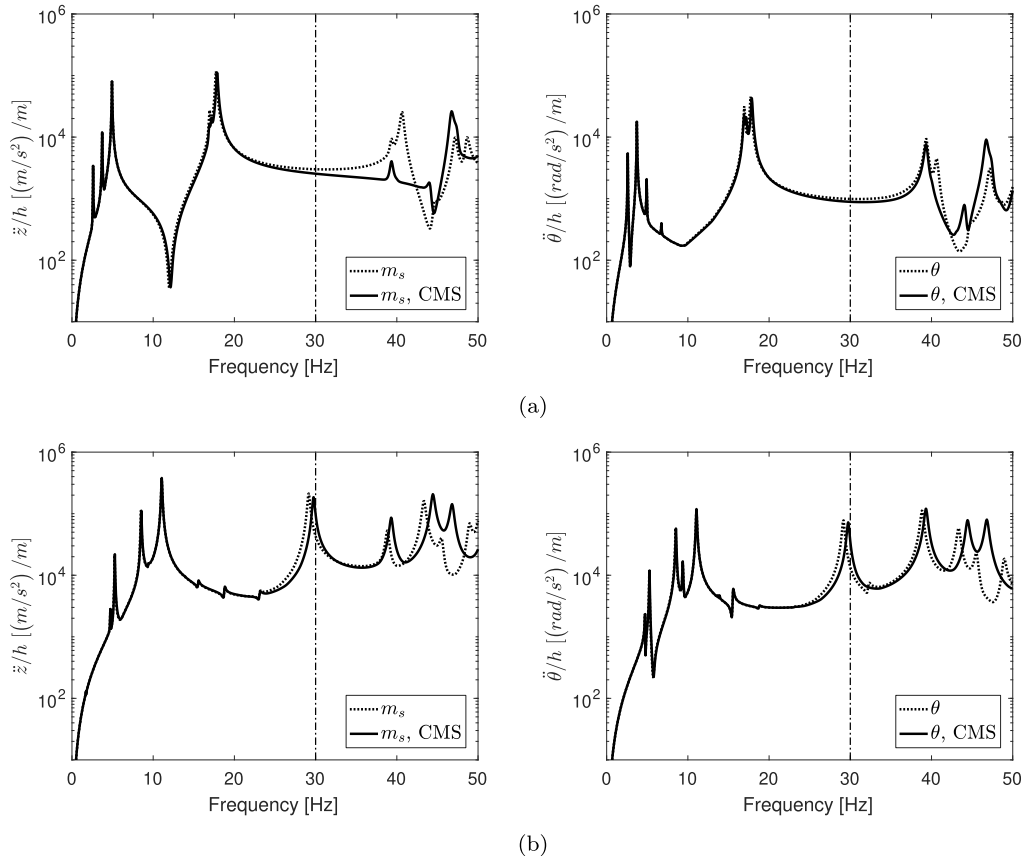
L. Dimauro, S. Venturini, A. Tota et al.

Fig. 13. MOR effect on vehicle model sprung mass FRFs: un-tracked vehicle (a) and tracked vehicle (b).
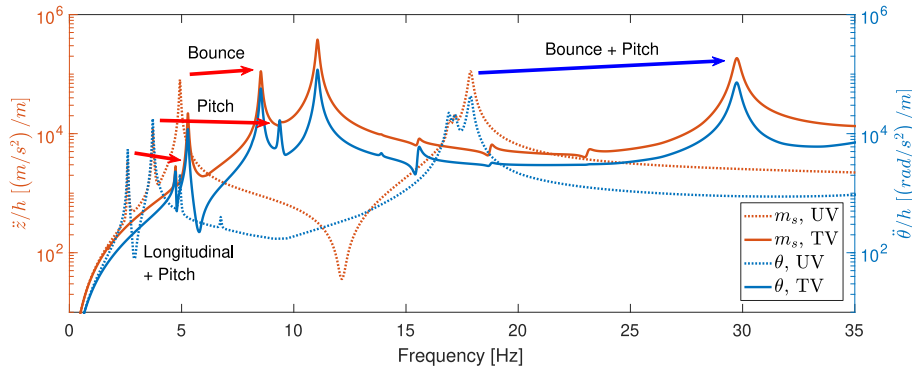

Fig. 14. Track coupling effect on vehicle models: sprung mass FRFs.

excitation emphasises the maximum theoretical response, in re-ality sprung mass bounce and pitch behaviours are excited simul-taneously. The modulation of comfort FRFs through wheelbase delays is called wheelbase filter. In Figs. 15 and 16, the wheelbase filter effects on comfort FRFs are shown.

The distance in frequency between the "demodulated arcs" in non-synchronous FRFs corresponds to the inverse of the delay τ_q at each input, previously computed to evaluate the delay vector in Eq. (23). Moreover, the FRF of the delayed excitation are at least tangent to the synchronous one in the CMS bandwidth of interest. The influence of wheelbase filter, in case of tracked vehicle is more evident in the FRFs of the unsprung masses in Fig. 16. The un-tracked vehicle road wheels are uncoupled each other, hence

their response is the unaffected by the longitudinal vehicle speed. Differently, for the tracked vehicle, unsprung mass FRFs have lower amplitudes at increasing longitudinal vehicle speed, since the track is coupling axles.

4.2. Time domain response

In this section, the time domain response of the vehicle on different road profiles is computed starting from the differential equations of the system in Eq. (15) using the CMS reduced models. The time domain response is computed using the state-space approach. The analysis is performed on three different tracks to verify the consistency of the CMS modal truncation, the coupling
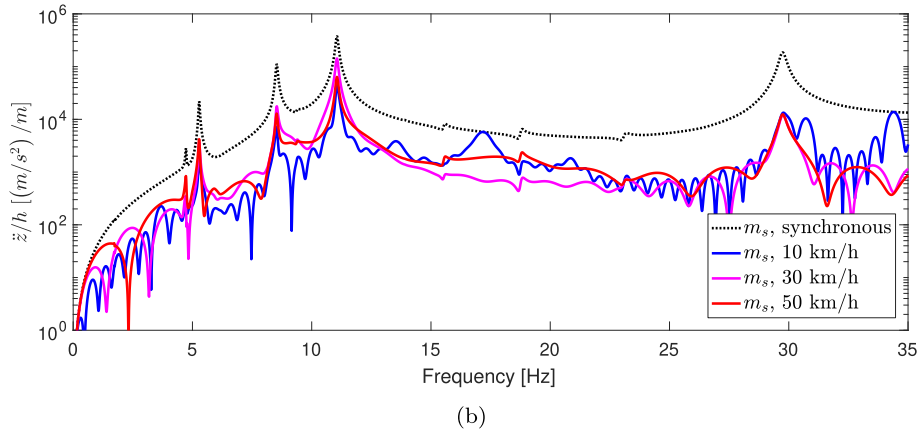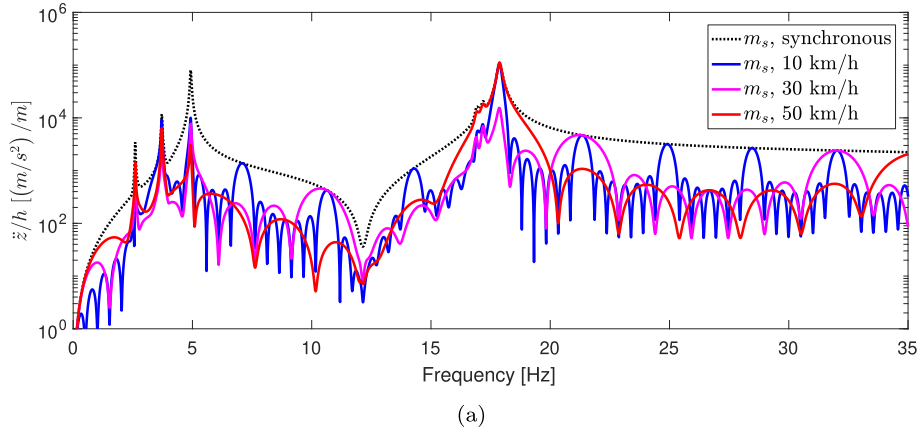
L. Dimauro, S. Venturini, A. Tota et al.

Fig. 15. Wheelbase filter on sprung mass vertical acceleration FRF: un-tracked vehicle (a) and tracked vehicle (b).
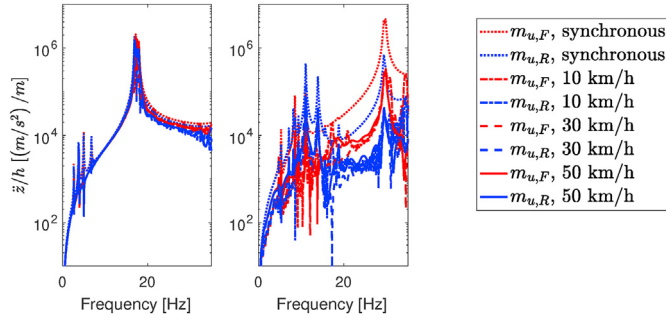

Fig. 16. Wheelbase filter on unsprung masses vertical acceleration FRFs: un-tracked vehicle (left) and tracked vehicle (right).

effect induced by the track on the sprung mass behaviour, and the effect of longitudinal vehicle speed on the sprung mass comfort. Moreover, the time domain analysis is focused on generalised displacements, since accelerations are strongly affected by terrain spectral content, not considered in the simplified modeling of the proposed tracks.

4.2.1. Tracks

The numerical analysis is performed on three longitudinal tracks inspired by road profiles available at Centro Polifunzionale di Sperimentazione (CePoliSpe) at Montelibretti Italian Army Center (Italy). All the tracks are 30 m long and 5 m wide and present initial and final sections completely flat. The vertical road profiles are sampled at 0.01 m resolution and a centered spatial moving

average on 0.2 m track length is implemented to avoid removable discontinuity. It follows the list of the tracks:

● *Long hill track*: it presents a 0.4 m tall hill 10 m long with entering and exiting 1 m long linear ramps. The track is approached at low speed to verify stationary displacement behaviour, and at high speed to validate CMS modal truncation bandwidth.

● *Separated waves track*: it presents a sinusoidal road profile of 0.15 m depth and 1.8 m of characteristic length, 10 full periods are present in the track. The track is used to show track coupling effect.

● *Out-of-phase (OOP) waves track, namely "Svergolatelai"*: it presents a sinusoidal road profile of 0.6 m depth and 1.2 m of characteristic length, with out-of-phase vertical excursion in the lateral direction, and it is approached by the vehicle with a lateral offset of 1 m. In this way, the vehicle torsional behaviour in longitudinal direction is excited, hence the structural integrity can be evaluated in critical conditions. The track is approached with a lateral offset, in such a way the vehicle barycentre is not centered with the track, hence sprung mass is vertically excited.

The three tracks are depicted in Fig. 17, where p is the track vertical profile, L and R subscripts indicate the left or right location of the profile, I and O subscripts indicate the coincidence with the centre of the inner or outer track pad row. Therefore, a total of four vertical profiles are imposed kinematics of the input DOFs of the vehicle model. In long hill and separated waves tracks the four curves are completely coincident as the road profile does not
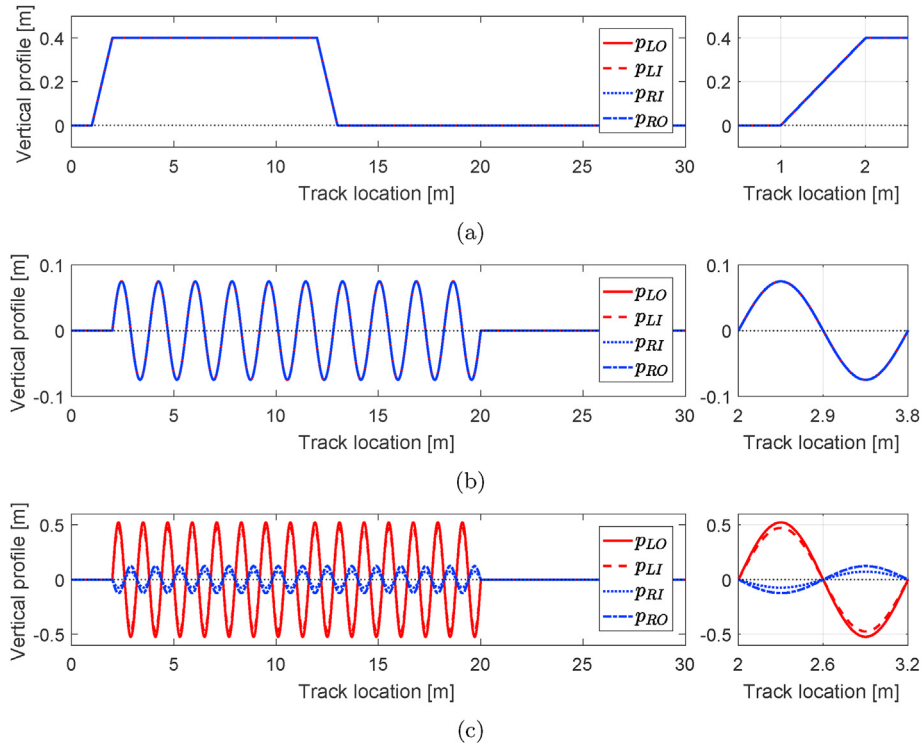
Fig. 17. Track vertical road profiles (left) and details (right): Long hill track (a), separated waves track (b), and OOP waves track with Y+ offset (c).

change laterally. Instead OOP waves track shows the out-of-phase behaviour between right and left profiles, the further variation between inner and outer track pads, and also the different amplitude since lateral offset of the vehicle.

4.2.2. Model order reduction approximation

The un-tracked vehicle model is tested against the long hill track at 5 km/h and 50 km/h to validate the CMS modal truncation bandwidth. The validation is limited to the un-tracked vehicle, since the low frequency modal content of the reduced model represents the worst case scenario with respect to the tracked vehicle.

Figs. 18 and 19 show the comparison of the full and CMS models of the un-tracked vehicle performing the long hill track.

In the first graph, the red and blue dashed curves represent the spatially delayed road profiles perceived by the front h_F and rear h_R axles, hence the spatial delay is the vehicle wheelbase. The graph shows in black the sprung mass m_s vertical displacement for different models and in different orange and cyan style curves, the front $m_{u,F}$ and the rear $m_{u,R}$ unsprung mass vertical displacements. In the following graph, the sprung mass vertical acceleration is shown, while n the latter graph the roll angle φ and the pitch angle θ of the sprung mass are shown.

Fig. 18 shows the gradual increment of sprung mass displacement as the un-tracked vehicle approaches the hill. Since the slow speed, the sprung mass does not show a strong overshoot of response with respect to the entering and exiting ramps. The vertical displacement in stationary condition is consistent on the hill, i.e., 7−12 m of track location. The sprung mass vertical acceleration shows positive and negative acceleration peaks corresponding to each axle entering and exiting the ramps with a maximum vertical acceleration modulus of about 6 m/s². Finally, the maximum sprung mass pitch of 6° is consistent with the static condition.

Instead, Fig. 19 shows the behaviour of un-tracked vehicle approaching the long hill at high speed. Both the sprung and unsprung masses have considerable overshoot entering and exiting the hill with a significant unsprung mass overshoot of about 0.1 m. Differently from low speed case, the unsprung mass displacement is steeper than the input profile as a consequence of inertial contribution in the transient behaviour. The sprung mass vertical acceleration reaches maximum modulus peak of about 75 m/s². Moreover, the sprung mass pitch is consistently larger than low speed case one.

In both cases, the un-tracked model results are completely consistent to full model results.

4.2.3. Track chain coupling effect

In this section, the CMS models of un-tracked (UV) and tracked (TV) vehicles are compared and the contribution of track chain coupling in vertical vehicle dynamics is shown to be significant. In all the cases the longitudinal vehicle speed is 30 km/h.

In Fig. 20, it is shown the marginal contribution on sprung mass vertical displacement of the track chain coupling. Instead, the wide overshoots of front unsprung mass and undershoots of rear unsprung mass are fundamentally caused by the track connection through axles. Consequently, the TV sprung mass vertical acceleration is much higher than UV. The coupling of axles even affects the sprung mass pitch angle which is marginally higher in TV case.

In Fig. 21, the separated waves track is approached. From the vertical displacement graph, it is possible to notice the track has a filtering effect on the unsprung mass vertical displacements, while negligible on sprung mass, which is simply out-of-phase. As before, the track coupling is not beneficial for TV sprung mass vertical acceleration which is higher than UV. Also, sprung mass pitch is marginally affected.

In Fig. 22, the OOP waves track is approached. As for previous tracks, the track coupling is filtering the unsprung mass vertical displacements, and increasing the sprung mass accelerations. Instead, larger roll angles are observed and are significantly
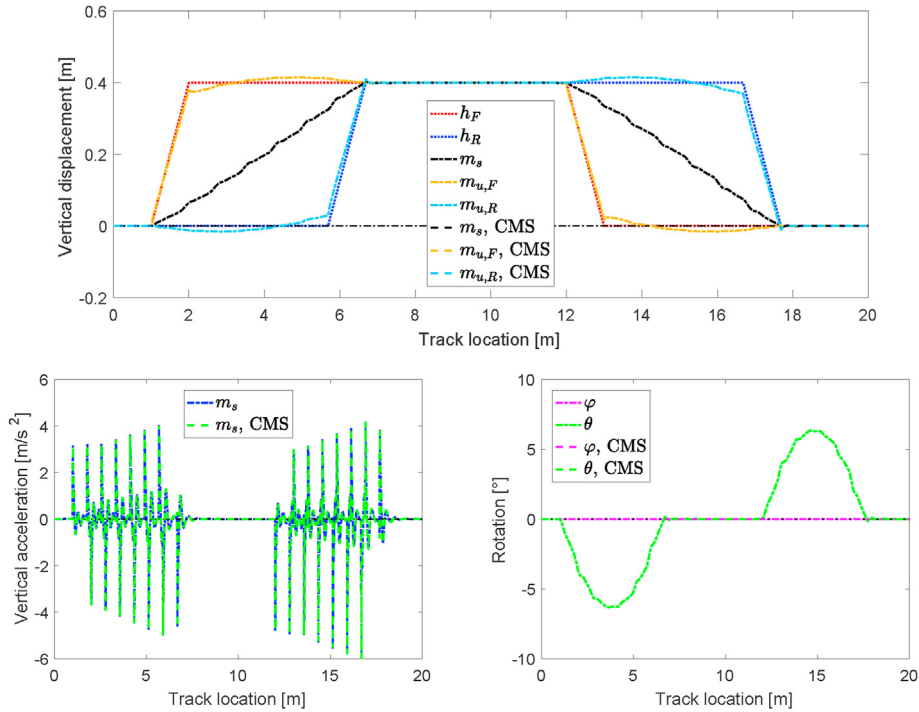
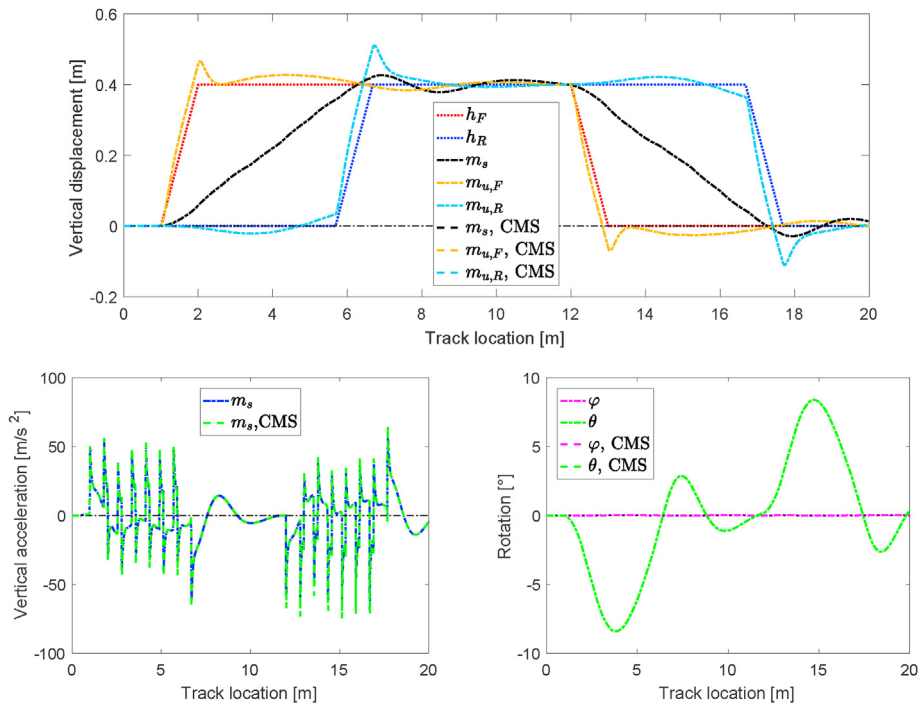**Fig. 18.** MOR effect on un-tracked vehicle model: long hill track at 5 km/h.

Fig. 19. MOR effect on un-tracked vehicle model: long hill track at 50 km/h.

described by the tracked vehicle model.

4.2.4. Longitudinal speed effect

In this section, the longitudinal vehicle speed is changed to study the contribution on vertical CMS tracked model dynamics.

In Fig. 23, the long hill track is approached. The increase of speed slightly increase the amplitude of vertical displacements, while strongly affects sprung mass acceleration. Also, sprung mass pitch behaviour is marginally increased by speed.

Similar behaviour occurs in Fig. 24 approaching the separated waves track. The speed increases vertical displacements and vertical accelerations. Wide effect occurs on sprung mass pitch.
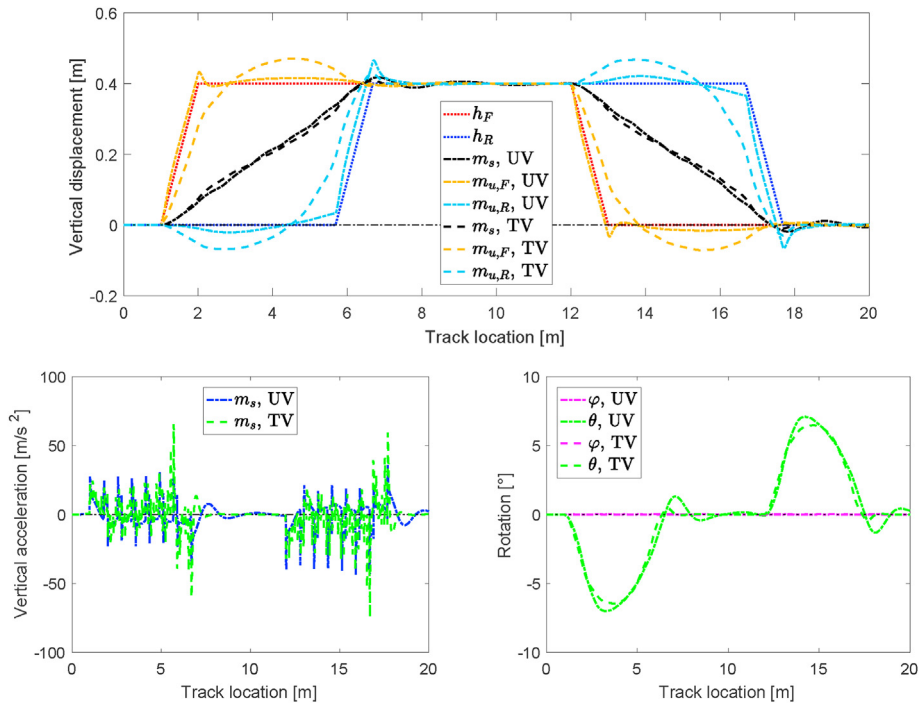
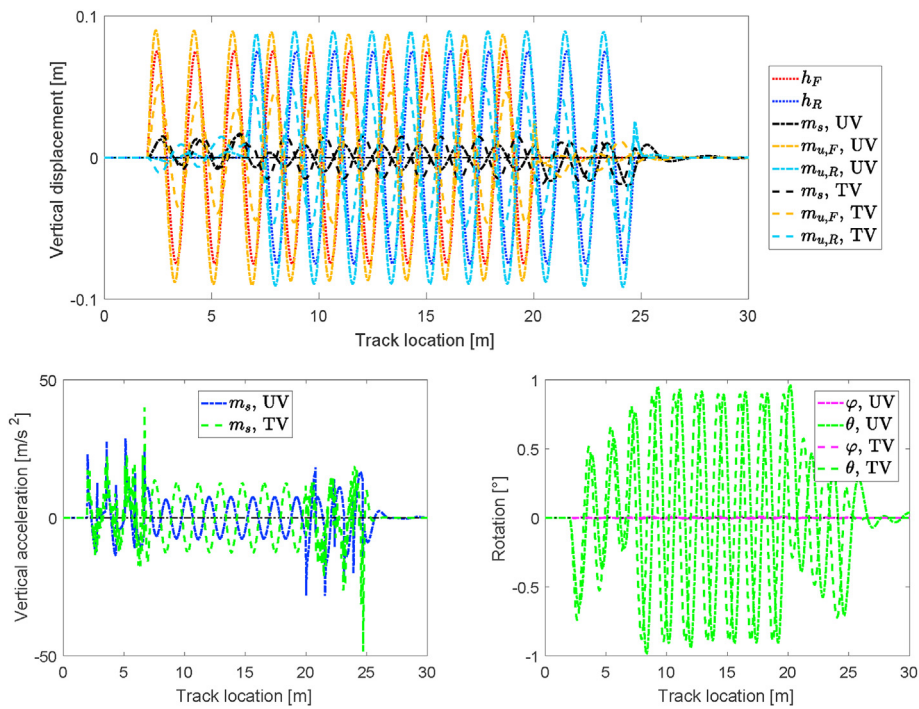**Fig. 20.** Track chain coupling effect on tracked vehicle CMS model: long hill track.

Fig. 21. Track chain coupling effect on tracked vehicle CMS model: separated waves track.

5. Conclusions

In this paper, the high-speed tracked vehicle vertical comfort dynamics is approached by using a model order reduction technique.

The vehicle comfort is studied in small oscillations regime through the development of a linear model in which the stiffness of the track assembly is experimentally evaluated.

The model has been strongly reduced to lower the computational costs: the final track assembly FEM model has a number of DOFs four orders of magnitude less than the active DOFs of the initial model. Similarly, the tracked vehicle model, presenting hundreds of track assemblies connected to the axles, has been further reduced with CMS technique up to 2.4% of the full vehicle
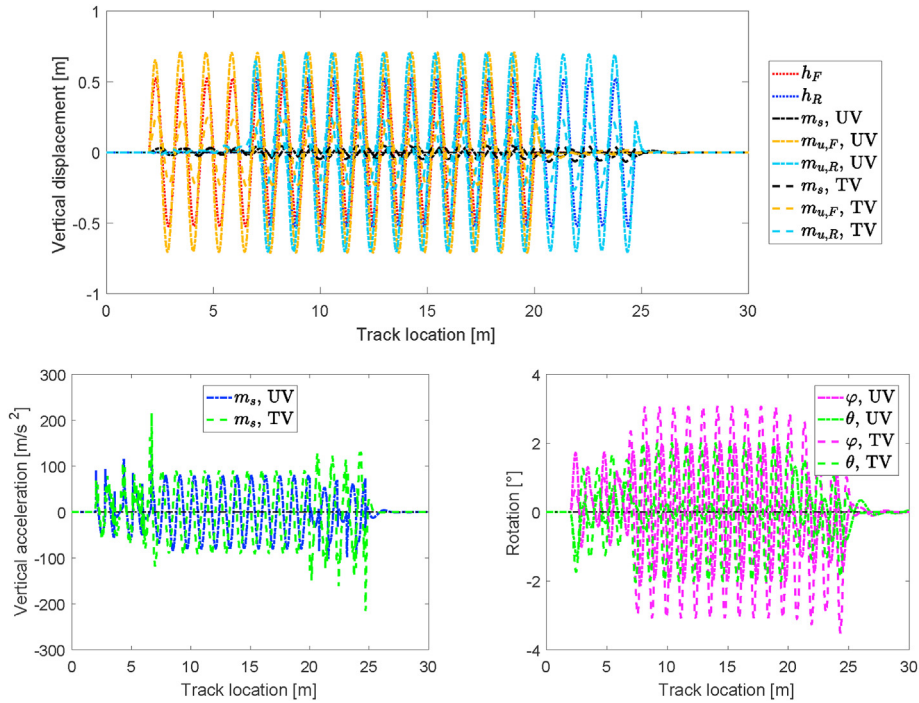
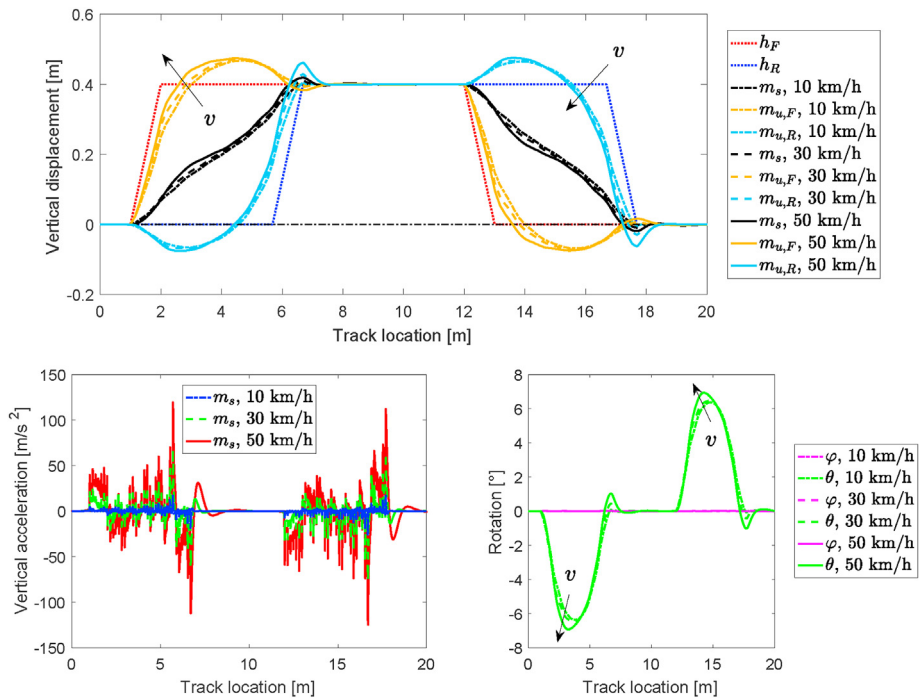**Fig. 22.** Track chain coupling effect on tracked vehicle CMS model: out-of-phase waves + shift track.

Fig. 23. Longitudinal speed effect on tracked vehicle CMS model: long hill track.

model. The final CMS tracked vehicle uses only 402 DOFs to properly depict the comfort behaviour, requiring fractions of second to perform time domain analysis of 30 m long track at low speed.

The comparison of un-tracked and tracked vehicle models shows the necessity of the track chain in the comfort analysis. In frequency domain, the sprung and unsprung mass natural frequencies are drastically increased, due to the additional track assembly stiffness which outlasts the additional inertial contribution. The wheelbase filtering effect is amplified by the track chain presence, increasing the margins for sprung mass comfort. In time domain, from evaluations on several tracks, the track chain has a strong filtering effect on vertical displacement of unsprung masses. Furthermore, the track chain couples axles on the same side, which is a critical issue for the roll behaviour of the sprung mass.
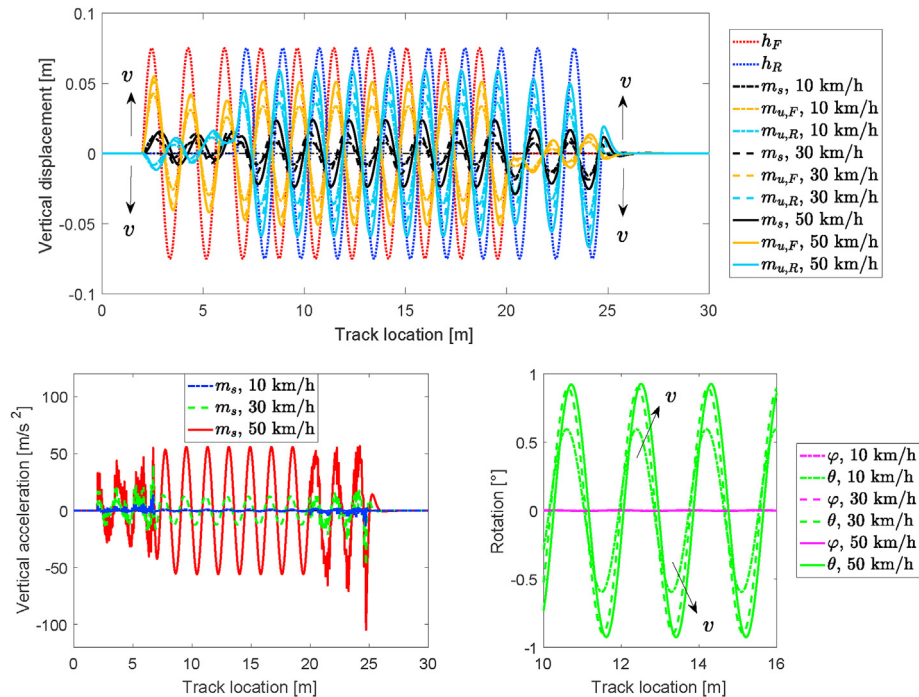
Fig. 24. Longitudinal speed effect on tracked vehicle CMS model: separated waves track.

In future developments of this research, the linear track assembly stiffness could be substituted by the nonlinear experimental characteristics. Meanwhile, non-holonomic interactions between the ground and track chain input DOFs, to also depict loss of contact, could be introduced, as well. Finally, the introduction of soft soil model can improve the capability of the model to supply significant information to tracked vehicle comfort also extendable to sprung mass accessory features as pointing devices and sensors.

Acknowledgement

References

[1] Dudziński PA, Chołodowski J. A method for predicting the internal motion resistance of rubber-tracked undercarriages, pt. 1. a review of the state-of-the-art methods for modeling the internal resistance of tracked vehicles. J Terramechanics 2021;96:81–100. https://doi.org/10.1016/j.jterra.2021.02.006.

[2] Ruslan NAI, Amer NH, Hudha K, Kadir ZA, Ishak SAFM, Dardin SMFS. Modelling and control strategies in path tracking control for autonomous tracked vehicles: a review of state of the art and challenges. J Terramechanics 2023;105:67–79. https://doi.org/10.1016/j.jterra.2022.10.003.

[3] Tota A, Dimauro L, Velardocchia F, Paciullo G, Velardocchia M. An intelligent predictive algorithm for the anti-rollover prevention of heavy vehicles for off-road applications. Machines 2022;10(10):835. https://doi.org/10.3390/machines10100835.

[4] Wong J. Dynamics of tracked vehicles. Veh Syst Dyn 1997;28(2–3):197–219. https://doi.org/10.1080/00423119708969354.

[5] Keays RH. Analysis of armoured-vehicle track loads and stresses, with considerations on alternative track materials. Materials Research Laboratory ASCOT VALE (AUSTRALIA); 1989.

[6] Ma Z-D, Perkins N. A track-wheel-terrain interaction model for dynamic simulation of tracked vehicles. Veh Syst Dyn 2002;37(6):401–21. https://doi.org/10.1076/vesd.37.6.401.3522.

[7] McCullough MK, Haug EJ. Dynamics of high mobility track vehicles. J Mech Design, Trans ASME 1986;108:189–96. https://doi.org/10.1115/1.3260801.

[8] Ma ZD, Perkins NC. A super-element of track-wheel-terrain interaction for dynamic simulation of tracked vehicles. Multibody Syst Dyn 2006;15:347–68. https://doi.org/10.1007/s11044-005-9001-3.

[9] Wang P-x, Rui X-t, Yu H-l, Wang G-p, Chen D-y. Adaptive control of track

[10] Dhir A, Sankar S. Analytical track models for ride dynamic simulation of tracked vehicles. J Terramechanics 1994;31(2):107–38. https://doi.org/10.1016/0022-4898(94)90010-8.

[11] Dhir A, Sankar S. Assessment of tracked vehicle suspension system using a validated computer simulation model. J Terramechanics 1995;32(3):127–49. https://doi.org/10.1016/0022-4898(95)00012-7.

[12] Dhir A, Sankar S. Ride dynamics of high-speed tracked vehicles: simulation with field validation. Veh Syst Dyn 1994;23(1):379–409.

[13] Gniłka J, Mkeżyk A. Experimental identification and selection of dynamic properties of a high-speed tracked vehicle; [identyfikacja doświadczalna oraz dobór cech dynamicznych układu jezdnego szybkobieżnego pojazdu gkasienicowego]. Eksploatacja i Niezawodnosc 2017;19(1):108–13. https://doi.org/10.17531/ein.2017.1.15.

[14] Janarthanan B, Padmanabhan C, Sujatha C. Longitudinal dynamics of a tracked vehicle: simulation and experiment. J Terramechanics 2012;49(2):63–72. https://doi.org/10.1016/j.jterra.2011.11.001.

[15] Venkatasubramanian N, Banerjee S, Balamurugan V. Non-linear seventeen degrees of freedom ride dynamics model of a full tracked vehicle in simmechanics. Procedia Eng 2016;144:1086–93. https://doi.org/10.1016/j.proeng.2016.05.067.

[16] Banerjee S, Balamurugan V, Krishnakumar R. Ride comfort analysis of math ride dynamics model of full tracked vehicle with trailing arm suspension. Procedia Eng 2016;144:1110–8. https://doi.org/10.1016/j.proeng.2016.05.074.

[17] Campanelli M, Shabana AA, Choi JH. Chain vibration and dynamic stress in three-dimensional multibody tracked vehicles. Multibody Syst Dyn 1998;2:277–316.

[18] Ryu HS, Bae DS, Choi JH, Shabana AA. A compliant track link model for high-speed, high-mobility tracked vehicles. Int. J. Numer. Meth. Engng 2000;48:1481–502.

[19] Bonisoli E, Lisitano D, Dimauro L. Experimental and numerical mode shape tracing from components to whole motorbike chassis. In: Moens D, Desmet W, Pluymers B, Rottiers W, editors. International conference on noise and vibration engineering - ISMA-USD2018. Leuven (Be): KU Leuven - Departement Werktuigkunde; 2018. p. 3597–604.

[20] Bonisoli E, Lisitano D, Dimauro L, Peroni L. A proposal of dynamic behaviour design based on mode shape tracing: numerical application to a motorbike frame. In: Linderholt A, Allen MS, Mayes RL, Rixen D, editors. Dynamic substructures, ume 4. Cham: Springer International Publishing; 2020. p. 149–58. https://doi.org/10.1007/978-3-030-12184-6_14.

[21] Bonisoli E, Lisitano D, Dimauro L. Detection of critical mode-shapes in flexible multibody system dynamics: the case study of a racing motorcycle. Mech Syst Signal Process 2022;180:109370. https://doi.org/10.1016/j.ymssp.2022.109370.

[22] Bonisoli E, Vella AD, Venturini S. Uncertainty effects on bike spoke wheel

modal behaviour. In: Conference Proceedings of the Society for Experimental Mechanics Series. Springer; 2023. p. 111–23. https://doi.org/10.1007/978-3-031-04090-0_13.

[23] Balamurugan S, Srinivasan R. Tracked vehicle performance evaluation using multi body dynamics. Defence Sci J 2017;67(4):476. https://doi.org/10.14429/dsj.67.11534.

[24] Rubinstein D, Hitron R. A detailed multi-body model for dynamic simulation of off-road tracked vehicles. J Terramechanics 2004;41(2–3):163–73. https://doi.org/10.1016/j.jterra.2004.02.004.

[25] Grazioso A, Ugenti A, Galati R, Mantriota G, Reina G. Modeling and validation of a novel tracked robot via multibody dynamics. Robotica 2023;41(10):3211–32. https://doi.org/10.1017/S0263574723000966.

[26] Nicolini A, Mocera F, Somà A. Multibody simulation of a tracked vehicle with deformable ground contact model. Proc Inst Mech Eng - Part K J Multi-body Dyn 2019;233:152–62. https://doi.org/10.1177/1464419318784293.

[27] Ugenti A, Galati R, Mantriota G, Reina G. Kinematic modelling of a high mobility tracked robot. In: The international conference of IFToMM Italy. Springer; 2022. p. 37–44. https://doi.org/10.1007/978-3-031-10776-4_5.

[28] Venturini S, Bonisoli E, Rosso C, Velardocchia M. A tyre-rim interaction digital twin for biaxial loading conditions. Mech Mach Theor 2024;191:105491. https://doi.org/10.1016/j.mechmachtheory.2023.105491.

[29] Venturini S, Rosso C, Velardocchia M. An automotive steel wheel digital twin for failure identification under accelerated fatigue tests. Engineering Failure Analysis 2024;158:107979. https://doi.org/10.1016/j.engfailanal.2024.107979.

[30] Kciuk S, Mkeżyk A. Modelling of tracked vehicle dynamics. Journal of KONES 2010;17(1):223–32.

[31] Mezyk A, Switonski E, Kciuk S, Klein W. Modelling and investigation of dynamic parameters of tracked vehicles. Mechanics and Mech Eng 2011;15(4):115–30.

[32] Z. Hryciów, P. Rybak, Numerical research of the high-speed military vehicle track, AIP conference proceedings 2078. doi:10.1063/1.5092032.

[33] Meywerk M, Fortmüller T, Fuhr B, Baß S. Real-time model for simulating a tracked vehicle on deformable soils. Adv Mech Eng 2016;8:1–14. https://doi.org/10.1177/1687814016647889.

[34] Wang C, Zhang W, Wang G, Guo Y. Research on a high power density mechanical-electrical-hydraulic regenerative suspension system for high-speed tracked vehicles. In: Proceedings of the institution of mechanical engineers, Part D: journal of automobile engineering, vol. 236; 2022. p. 2711–24. https://doi.org/10.1177/09544070211061010. 12.

[35] Lacombe J, Moran M, Happel S. A 3-dimensional dynamics model for generating tracked vehicle seismic signals. In: Proc. 2000 meeting of the military sensing symposia (MSS); 2000. p. 1–7.

[36] Solomon U, Padmanabhan C. Hydro-gas suspension system for a tracked vehicle: modeling and analysis. J Terramechanics 2011;48(2):125–37. https://doi.org/10.1016/j.jterra.2010.12.001.

[37] Caldeira AB, de Carvalho MS, da Costa Neto RT. Estimation of tracked vehicle suspension parameters. Acta Sci Technol 2017;39(1):51–7. https://doi.org/10.4025/actascitechnol.v39i1.29385.

[38] Jothi S, Balamurugan V, Mohan KM. Ride dynamics of a tracked vehicle with a finite element vehicle model. Defence Sci J 2016;66:19–25. https://doi.org/10.14429/dsj.66.9201.

[39] Kotiev G, Miroshnichenko A, Stadukhin A, Kositsyn B. Determination of mechanical characteristics of high-speed tracked vehicles traction motor with individual drive wheels. In: Journal of physics: conference series, vol. 1177.

[40] Paddan GS, McIlraith ML. Noise and vibration measurements in a viking military vehicle. Defence Technol 2021;17(6):1976–87. https://doi.org/10.1016/j.dt.2020.09.021.

[41] Velardocchia M, Bonisoli E, Tota A, Lisitano D, Paciullo G, Trevisi M. PSD profiles for dynamic and durability tests of military off-road vehicle racks. SAE Technical Papers 2023:1–8. https://doi.org/10.4271/2023-01-0107.

[42] Zhao H, Wang G, Wang H, Bi Q, Li X. Fatigue life analysis of crawler chain link of excavator. Eng Fail Anal 2017;79:737–48. https://doi.org/10.1016/j.engfailanal.2017.04.034.

[43] Mars WV, Ostberg D. Fatigue damage analysis of an elastomeric tank track component. In: 2012 SIMULIA community COMFERENCE; 2012. p. 1–14.

[44] Rovarino D, Actis Comino L, Bonisoli E, Rosso C, Venturini S, Velardocchia M, et al. Hardware and virtual test-rigs for automotive steel wheels design. SAE Technical Papers 2020:1–9. https://doi.org/10.4271/2020-01-1231.

[45] Wong J, Chiang C. A general theory for skid steering of tracked vehicles on firm ground. In: Proceedings of the institution of mechanical engineers, Part D: journal of automobile engineering, vol. 215; 2001. p. 343–55. https://doi.org/10.1243/0954407011525683. 3.

[46] Özdemir MN. Steering dynamics of tracked vehicles, ph.D. Thesis, yüksek lisans tezi, orta doğu teknik üniversitesi. Fen Bilimleri Enstitüsü; 2016.

[47] Tang S, Yuan S, Hu J, Li X, Zhou J, Guo J. Modeling of steady-state performance of skid-steering for high-speed tracked vehicles. J Terramechanics 2017;73:25–35. https://doi.org/10.1016/j.jterra.2017.06.003.

[48] Zhai L, Zhang X, Wang Z, Mok YM, Hou R, Hou Y. Steering stability control for four-motor distributed drive high-speed tracked vehicles. IEEE Access 2020;8:94968–83. https://doi.org/10.1109/ACCESS.2020.2995520.

[49] Tota A, Velardocchia M, Rota E, Novara A. Steering behavior of an articulated amphibious all-terrain tracked vehicle. SAE Technical Papers 2020:1–11. https://doi.org/10.4271/2020-01-0996.

[50] Tota A, Velardocchia M, Rota E, Novara A. Articulated steering control for an all-terrain tracked vehicle. In: Advances in Italian mechanism science: proceedings of the 3rd international conference of IFToMM Italy 3. Springer; 2021. p. 823–30. https://doi.org/10.1007/978-3-030-55807-9_91.

[51] Tota A, Galvagno E, Velardocchia M. Analytical study on the cornering behavior of an articulated tracked vehicle. Machines 2021;9(2):38. https://doi.org/10.3390/machines9020038.

[52] D. P. International, Ajax armoured vehicle problems and what happens next, (Date accessed: 20/12/2023). URL https://www.defenceprocurementinternational.com/features/land/has-the-troubled-ajax-armoured-vehicle-programme-turned-a-page.

[53] Bonisoli E, Dimauro L, Venturini S. Lupos: open-source scientific computing in structural dynamics. In: Conference Proceedings of the Society for Experimental Mechanics Series. Springer; 2023. 177–88. https://doi.org/10.1007/978-3-031-34946-1_23.

[54] Craig RR, Bampton MCC. Coupling of substructures for dynamic analyses. AIAA J 1968;6(7):1313–9. https://doi.org/10.2514/3.4741.

[55] Allemang RJ. A correlation coefficient for modal vector analysis. In: Proc. Of the 1st IMAC; 1982. 110–16.

[56] Bonisoli E, Delprete C, Rosso C. Proposal of a modal-geometrical-based master nodes selection criterion in modal analysis. Mech Syst Signal Process 2009;23(3):606–20. https://doi.org/10.1016/j.ymssp.2008.05.012.